NASA Technical Memorandum 100493

A VECTOR-BASED FAILURE DETECTION AND ISOLATION ALGORITHM FOR A DUAL FAIL-OPERATIONAL REDUNDANT STRAPDOWN INERTIAL MEASUREMENT UNIT

(NASA-TM-100493) A VECTOR-BASED FAILURE DETECTION AND ISOLATION ALGORITHM FOR A DUAL FAIL-OPERATIONAL REDUNDANT STRAPDOWN INERTIAL MEASUREMENT UNIT (NASA) 46 p
N87-29531
Unclas
Avail: NTIS HC A03/MF A01 CSCL 01D G3/06 0100029

FREDERICK R. MORRELL AND
MELVIN L. BAILEY

SEPTEMBER 1987

NASA
National Aeronautics and Space Administration
Langley Research Center
Hampton, Virginia 23665

SUMMARY

A vector-based failure detection and isolation technique, which can provide dual fail-operational capability for a redundant strapdown inertial measurement unit over all aircraft operating environments, is developed. The inertial sensors are skewed in a semi-octahedral array of four two degree-of-freedom gyros and accelerometers. Failure detection is based on comparison of parity equations with a threshold, and isolation is based on comparison of logic variables which are keyed to pass/fail results of the parity test.

Since the inertial measurement unit provides flight control, display, and navigation data, a multi-level approach to failure detection is used to ensure adequate coverage for these avionics functions. Sensor error models are introduced to expose the susceptibility of the parity equations to sensor errors and physical separation effects such as lever-arm acceleration. The threshold function, which is comprised of static and dynamic sensor errors and separation effect compensation terms, is derived for accelerometers. The failure detection and isolation algorithm is evaluated in a simulation of a commercial transport operating in a range of light to severe turbulence environments. A bias-jump failure level of 0.2 deg/hr inserted in the gyro data was detected and isolated properly in the light and moderate turbulence environments, but not detected in the extreme turbulence environment. An accelerometer bias-jump failure level of 1.5 milli-g was detected over all turbulence environments. For both types of inertial sensor, hard-over and null type failures were detected in all environments without incident. The algorithm functioned without false alarm or false isolation over all turbulence environments for the runs tested. Dual fail-operational capability for the redundant strapdown inertial measurement unit was demonstrated with the use of the algorithm.

INTRODUCTION

Integrated avionics concepts for commercial aircraft use strapdown inertial sensors for angular rate and linear acceleration measurements for generation of aircraft states for guidance and control laws, display, and navigation systems. To meet safety and reliability requirements triply redundant IMU's have been used in the design of operational systems. Future aircraft designs, however, will stress maximum efficiency through relaxed static stability and require flight crucial information from the inertial sensors for integrated avionics functions. Reliability and safety issues for these aircraft will mandate automatic selection of operational sensors with quick rejection of failed components so that flight control, display, or navigation functions will not be impaired. Accordingly, research at NASA Langley Research Center has been directed toward fault tolerant concepts for inertial sensor arrays. Cost considerations, however, restrict the system complexity and number of inertial sensors available to generate required flight crucial data. This implies the use of an optimum geometric array of sensors with efficient failure detection and isolation (FDI) and redundancy management (RM) algorithms to satisfy reliability and safety requirements (ref. 1). The purpose of this paper is to report on the development of a vector-based technique for redundancy management of a

skewed array of inertial sensors to enable a fail-operational/fail-operational/fail-safe capability meeting appropriate reliability and safety requirements.

To develop and evaluate redundancy management algorithms, Langley Research Center has designed and built an experimental, redundant strapdown inertial measurement unit (RSDIMU). The unit consists of a separable and communicating semi-octahedral array of four two degree-of-freedom (TDOF) gyros and four TDOF accelerometers (ref. 2). Because of widely varying reliability and performance requirements among the flight control, display, and navigation systems, and to account for a wide variety of sensor uncertainties and anomalies, this FDI design has been based on a multi-level structure (ref. 3). Accordingly, this report will show the development of a multi-level FDI algorithm which will provide dual fail-operational performance capability for the RSDIMU for flight control, display, and navigation systems.

The detection and isolation of failures of the separated RSDIMU is accomplished by comparing a function of the sensor outputs against a threshold. For failures which affect flight control, comparing a function of the sensor outputs against a threshold is sufficient. For systems requiring more accurate sensor data, such as display and navigation functions, the process is more complicated. That is, the failure thresholds must be compensated for normal sensor errors, such as scale factor and misalignment errors, which are large during aircraft maneuvers; also separation effect terms, such as lever-arm acceleration differences between sensors must be compensated for. In references 4 and 5 techniques are discussed for the generation of thresholds to account for the effects of dynamic sensor errors and sensor separation. A technique to provide separation effect compensation was developed in reference 6; however, it does not provide dual fail-operational capability. These analyses were performed for a limited range of sensor error and disturbance environment and considered a least-squares based FDI algorithm. The threshold compensation for separation effects offered in references 4 and 6, furthermore could lead to high false alarm rate and consequently to system failure. An alternative approach to threshold compensation for separation effects and hence to reliable dual fail-operational capability in the context of a vector-based FDI algorithm is offered in this paper.

This paper presents a description of the RSDIMU, an overview of the multi-level FDI concept, inertial sensor error models, and development of the vector-based FDI algorithm. The FDI capability of the algorithm is evaluated with the use of a digital simulation of a commercial transport over a range of turbulent environments.

SYMBOLS

A_i	logical variable for accelerometer failure isolation, $i = 1,2,3,4$
a_x, a_y, a_z	lateral, longitudinal, and normal body axes linear inertial accelerations, $(ft/s)^2$

a_i^B	resolution of accelerometer output in body coordinates, B = x,y,z; i = 1,2,3,4, $(ft/s)^2$
C_i	direction cosine matrix element, (i=1,2,3), rad
Dt	computation time interval, s
e_{ij}	edge vector relating ith to jth instruments, j>i; i = 1,2,3
F_{grav}	vector of vehicle body axes gravitational forces, ft/s^2
H	location parameter matrix, rad
g	acceleration due to gravity, $(ft/s)^2$
l_x, l_y, l_z	distance from vehicle cg to sensor location, ft
L_{ij}	logical variable for isolation of failed sensor
m	sensor output, rad, ft/s
n	number of sensors
$p_{a_{ijk}}$	edge vector parity equation residual relating ith and jth accelerometers, k = h, or s for hard-, or soft-range, ft/s
$p_{g_{ijk}}$	edge vector parity residual relating ith and jth gyros, k = h, m, or s for hard-, medium-, or soft-range, rad
$s_{a_{ki}}$	accelerometer measurement output, i = 1,2,3,4; k = x,y;ft/s
$s_{g_{ki}}$	gyro measurement output, i = 1,2,3,4; k = x,y; rad
S_i	spin or pendulous axes of inertial sensor; i = 1,2,3,4
t	time, s
T	failure detection threshold, rad, or ft/s
δ_{g_i}	g sensitive bias, i = 1,2,3,4; rad/s/g
δ_{a_i}	differential separation effect, i = x,y,z, (ft/s^2)

$\delta s_{a_{ki}}$	accelerometer error, k = x,y; i = 1,2,3,4; ft/s
$\delta s_{g_{ki}}$	gyro error, k = x,y; i = 1,2,3,4; rad
δs_{a_m}	maximum or upper bound of accelerometer error, ft/s
ε	scale factor error, ppm
λ	bias error, rad/sec or ft/s^2
μ	misalignment error, rad
ω_x, ω_y, ω_z	body axes angular rates, rad/s

Subscripts

a	accelerometer
f	filtered value
g	gyro
cg	center of gravity
i, j, k	element number, row, or column of matrices
la	lever-arm
m	maximum or upper bound
s	spin/pendulous axes

Superscripts

B	body-axes components
T	transpose
^	least-squares estimate
-1	inverse

DESCRIPTION OF THE RSDIMU

The RSDIMU has a complement of four TDOF gyros and four TDOF accelerometers mounted in a semi-octahedral configuration (see fig. 1) such that dual fail-operational performance is possible (ref. 2). The spin-axes of the TDOF gyros and pendulous axes of the TDOF accelerometers, S_i, are normal to the faces of the semi-octahedron. The measurement axes of the

accelerometers, $s_{a_{xk}}$, $s_{a_{yk}}$, lie in the plane of the face and are oriented such that the bisector of the sensitive axes is perpendicular to the baseline of the semi-octahedron. The gyro and accelerometer sensitive axes are nominally collinear. Any two gyros or two accelerometers would constitute sufficient information to complete an orthogonal triad for angular rate or linear acceleration body frame solutions. The reference frame for the sensors shown in figure 1 is x (pitch), y (roll), and z (yaw); this constitutes the ENU reference frame commonly used in navigation. From figure 1 the coordinate transformation which relates the sensor measurement axes to the body axes is

$$H = \left[\begin{array}{ccc} -c1 & c2 & -c3 \\ c2 & -c1 & -c3 \\ c2 & c1 & -c3 \\ -c1 & -c2 & -c3 \\ \hline c1 & -c2 & -c3 \\ -c2 & c1 & -c3 \\ -c2 & -c1 & -c3 \\ c1 & c2 & -c3 \end{array}\right] \qquad (1)$$

where $c1 = (\sqrt{3} + 1)/2\sqrt{3}$, $c2 = (\sqrt{3} - 1)/2\sqrt{3}$, and $c3 = 1/\sqrt{3}$. The first two rows of this 8 x 3 matrix represents the direction cosines for sensor axes x1 and y1; from rows 3 and 4 the output of sensor 2 can be found, etc. The dashed line in the matrix H indicates the separation of the RSDIMU into halves: IMU1 (instruments 1 and 2) and IMU2 (instruments 3 and 4). In the ideal case the gyro and accelerometer direction cosines are the same. The 4 x 3 matrix H_s defines the ideal transformation from the gyro/accelerometer spin/pendulous axes (s_1, s_2, s_3, s_4) to the body frame (x,y,z) as

$$H_s = \left[\begin{array}{ccc} -c3 & -c3 & c3 \\ -c3 & c3 & c3 \\ \hline c3 & c3 & c3 \\ c3 & -c3 & c3 \end{array}\right] \qquad (2)$$

As shown in figure 2, the sensor data output of the RSDIMU is processed in four separate channels. The output of each sensor pair is compensated for errors using a micro-processor. The compensated data is then processed in four separate solutions. Each channel processes FDI and redundancy management (RM) algorithms to satisfy the dual fail-operational requirement on the system. This is followed by least-squares solutions of the outputs of two valid gyros and accelerometers in body axes, after which conventional algorithms for attitude, alignment, and navigation are processed. A least-squares solution for linear acceleration can be obtained from any two (or more) accelerometers from the expression

$$\hat{a} = (H^T H)^{-1} H^T m_a / Dt \qquad (3)$$

where m_a is the 4 x 1 sensor measurement vector formed from the two accelerometers used for the solution, and H is the 4 x 3 direction cosine matrix, obtained from equation (1), relating the sensor axes to the body frame for the same two accelerometers. The least-squares estimates are formed from two sensors in each of the channels (e.g. channel one uses sensors 1 and 2). If an accelerometer or gyro fails, the ordering of solution pairs in that channel is changed via the redundancy management algorithm.

FAILURE DETECTION AND ISOLATION CONCEPT

The role of fault tolerant algorithms to meet avionics systems' reliability and performance is illustrated in figure 3. The information from the skewed array of inertial sensors is first proved reliable before being passed to the flight control, display, or navigation algorithms. Since the sensors are skewed relative to the aircraft principal axes, FDI must be accomplished as a function of the sensor axes.

The purpose of the experimental RSDIMU is to provide a basis for the evaluation of FDI algorithms which provide the dual fail-operational capability necessary to satisfy reliability and performance requirements. To satisfy dual fail-operational requirements, the RSDIMU must be able to survive two accelerometer or gyro failures and cease operation after a third malfunction of either type of sensor is detected. Failure detection is accomplished with the use of parity equations which are linear combinations of the sensor outputs and which are compared to a failure threshold. The parity equations remove the quantities the sensors measure; thus they leave residuals which are composed of undesirable quantities. The parity equation residuals, therefore, are a function of the instrument uncompensated errors, noise, and quantization. If the sensors are physically separated, differences in sensed structural modes, vibration, and lever-arm acceleration would impact the parity residuals. Static and dynamic sensor errors and separation effects, which are normal (but undesirable) sensor outputs, would dictate the level of detectable failure unless properly compensated, since the detection of failures is accomplished by comparison of a function of the parity residuals to a threshold. Therefore, the generation of thresholds for both gyros and accelerometers, which compensate for dynamic sensor errors and separation effects, is a major consideration in FDI algorithm development.

For flight control purposes the failure detection process is simple; the parity residuals are merely compared to a constant level threshold. For the avionics functions which require greater accuracy, however, the process is more complicated. Figure 4 illustrates the flow of information applicable to the display and navigation FDI processes. The parity equations are formed from current sensor data, filtered and compared to a threshold. The threshold is formed from several contributions: 1) a constant to account for unattenuated noise and quantization levels in the residuals; 2) known sensor error statistics which can be estimated analytically, such as misalignment, scale factor, and biases; 3) a function of the parity residuals passed through a washout filter; and 4) undesirable low frequency residuals, such as lever-arm acceleration. Immediate past

values of sensor data are used to form the threshold function to preclude corruption caused by hard-failed sensors.

Since the FDI algorithm must be designed to cover sensor failures which affect flight control, display, and navigation functions, a baseline configuration to allow multi-level coverage has been established (ref. 3) as shown in figure 5. Unfiltered parity equations are processed at the sensor measurement rate (64 Hz) and compared to an uncompensated threshold to ensure the removal of hard-failed sensor data before vehicle controllability is affected. The same parity residuals are filtered to attenuate noise so that moderate- or soft-level failures which might affect display or navigation performance might be easily detected. Moderate-level failures are removed from the system quickly since a first-order lag with fast rise time is used to filter the residuals. A second-order filter or long time constant first-order filter is used in the soft-failure channel to enhance the detection of failures which affect the navigation function. The processing rates for these channels, 32 Hz, and 1 Hz, reflect the fact that mid- and soft-range failures can be tolerated for a longer period of time without serious effect on display or navigation performance; however, these rates and the filter time constants are design parameters.

INERTIAL SENSOR ERROR MODELS

The angular rate sensors used in the RSDIMU are TDOF dynamically tuned gyros (ref. 2). The first-order performance parameters, consistent with a moderate to low accuracy inertial navigation system (INS), are given in table I. The first-order uncompensated errors for the gyro include: g- and non-g sensitive biases, misalignment, and scale factor nonlinearities. An expression for the output of the x-axis of gyro 1 (not including the effects of quantization and noise) is

$$
\begin{aligned}
s_{g_{x1}} &= [-c1\cdot\omega_x + c2\cdot\omega_y - c3\cdot\omega_z]\cdot Dt + \delta s_{g_{x1}} \\
&= [-c1\cdot q + c2\cdot p - c3\cdot r + \lambda_{g_1} - \mu_{g_{11}}\cdot c1\cdot q + \mu_{g_{12}}\cdot c2\cdot p - \mu_{g_{13}}\cdot c3\cdot r \\
&\quad + \delta_{g_1}\cdot(-c1\cdot a_x + c2\cdot a_y - c3\cdot a_z)/g + \varepsilon_{g_1}\cdot(-c1\cdot q + c2\cdot p \\
&\quad - c3\cdot r)]\cdot Dt
\end{aligned}
\tag{4}
$$

where the Dt factor accounts for the gyro output (radians/cycle). The first three terms of equation (4) represent the output of a perfect gyro, and the remaining terms represent sensor error as indicated in table I. The input rates to the gyros include inertial rates and local disturbances.

Linear acceleration is measured by TDOF accelerometers. The performance parameters given in table I are consistent with the requirements of a moderate to low accuracy INS. An expression for the output of the x-axis of accelerometer 1 is

$$s_{a_{x1}} = [-c1 \cdot a_x + c2 \cdot a_y - c3 \cdot a_z] \cdot Dt + \delta s_{a_{x1}}$$

$$= [-c1 \cdot a_x + c2 \cdot a_y - c3 \cdot a_z + \lambda_{a_1} - \mu_{a_{11}} \cdot c1 \cdot a_x + \mu_{a_{12}} \cdot c2 \cdot a_y - \mu_{a_{13}} \cdot c3 \cdot a_z$$

$$+ \varepsilon_{a_1} \cdot (-c1 \cdot a_x + c2 \cdot a_y - c3 \cdot a_z)] \cdot Dt \qquad (5)$$

The first three terms of equation (5) represent the output of an ideal accelerometer, and the remaining terms represent uncompensated first-order errors of the type listed in table I.

POSITION DEPENDENT DYNAMICS

Because of vehicle safety considerations, it may be necessary to separate the RSDIMU sensors in halves to decrease the probability of loss of the entire RSDIMU in the event of damage (e.g. caused by fire, lightning, etc.) to the aircraft. This means that different levels of vibration, structural modes, and lever-arm accelerations will be experienced by the sensors. Unless properly compensated in the FDI process, these effects could reduce failure detection sensitivity particularly in the soft-range failure channel which affects navigation performance. The rigid body acceleration in terms of accelerometer location relative to the vehicle center of gravity (cg) is

$$a = \dot{v} + \omega \times v - F_g + \dot{\omega} \times l + \omega \times \omega \times l$$

The first three terms on the right side of this expression represent the acceleration at the vehicle cg, and the last two terms on represent lever-arm acceleration. Expansion of this equation yields

$$a_x = a_{x_{cg}} + \delta a_{x_{la}}$$

$$= a_{x_{cg}} - (\omega_y^2 + \omega_z^2) \cdot l_x + (\omega_y \cdot \omega_x - \dot{\omega}_z) * l_y + (\dot{\omega}_y + \omega_x \cdot \omega_z) \cdot l_z$$

$$a_y = a_{y_{cg}} + \delta a_{y_{la}}$$

$$= a_{y_{cg}} + (\dot{\omega}_z + \omega_x \cdot \omega_y) \cdot l_x - (\omega_x^2 + \omega_z^2) \cdot l_y + (\omega_z \cdot \omega_y - \dot{\omega}_x) \cdot l_z$$

$$a_z = a_{z_{cg}} + \delta a_{z_{la}}$$

$$= a_{z_{cg}} + (\omega_x \cdot \omega_z - \dot{\omega}_y) \cdot l_x + (\dot{\omega}_x + \omega_y \cdot \omega_z) \cdot l_y - (\omega_x^2 + \omega_y^2) \cdot l_z \qquad (6)$$

An expression for the difference of the position effects between IMU1 and IMU2 is given by

$$a_{x_2} - a_{x_1} = \delta a_x$$

$$= \delta a_{x_{la2}} - \delta a_{x_{la1}}$$

$$a_{y_2} - a_{y_1} = \delta a_y$$

$$= \delta a_{y_{la2}} - \delta a_{y_{la1}}$$

$$a_{z_2} - a_{z_1} = \delta a_z$$

$$= \delta a_{z_{la2}} - \delta a_{z_{la1}} \qquad (7)$$

The vehicle linear acceleration measured at the IMU1 and IMU2 locations by accelerometers 1 and 2, and accelerometers 3 and 4, respectively, may be obtained from equation (3); therefore, these solutions when differenced provide a measure of the separation effects between the IMU halves as indicated by equation (7). The method could be easily extended to include structural modes and vibration for both the gyros and the accelerometers (refs. 4,6).

VECTOR BASED FDI METHOD

Parity Equations

A technique to determine parity equations which are particularly suited to TDOF instruments has been developed (refs. 1,7). A set of six parity equations for the gyros or accelerometers of the RSDIMU is formed when pairs of instruments are compared along an edge of the semi-octahedron. An expression for the edge vectors is formed from the cross products of the sensor spin-axes as illustrated in figure 1 and using equation (2)

$$e_{ij} = (s_i \times s_j)/(|s_i \times s_j|) \qquad j>i;\ i = 1,2,3 \qquad (8)$$

The accelerometer parity equations for the vector-based method are defined as the dot product

$$p_{a_{ij}} = [(a_i^B - a_j^B)\cdot e_{ij}]\cdot Dt \qquad j>i;\ i = 1,2,3 \qquad (9)$$

where a_i^B and a_j^B are the outputs of the ith and jth accelerometers expressed in body axes. When expanded, this expression becomes

$$
\begin{aligned}
p_{a_{12}} &= 1/\sqrt{2}\cdot(a_2^x - a_1^x + a_2^z - a_1^z)\cdot Dt \\
p_{a_{13}} &= 1/\sqrt{2}\cdot(a_3^x - a_1^x + a_1^y - a_3^y)\cdot Dt \\
p_{a_{14}} &= 1/\sqrt{2}\cdot(a_1^y - a_4^y + a_1^z - a_4^z)\cdot Dt \\
p_{a_{23}} &= 1/\sqrt{2}\cdot(a_2^y - a_3^y + a_3^z - a_2^z)\cdot Dt \\
p_{a_{24}} &= 1/\sqrt{2}\cdot(a_2^x - a_4^x + a_2^y - a_4^y)\cdot Dt \\
p_{a_{34}} &= 1/\sqrt{2}\cdot(a_3^x - a_4^x + a_4^z - a_3^z)\cdot Dt
\end{aligned}
\qquad (10)
$$

To express the quantity a_i^B in terms of sensor output, use equation (1) to obtain

$$
a_i^B = [H^T\cdot s_{a_{ki}}]/Dt \qquad k = x,y;\ i = 1,2,3,4
$$

where H^T is the 3 x 2 matrix corresponding to the ith accelerometer as given by equation (1). This expression can be used to obtain the parity equations in terms of sensor measurements. To get the parity residuals in terms of sensor errors and separation effects, substitute equation (5) for the sensor measurements taking care to account for sensor location (see the appendix for details). The results are

$$
\begin{aligned}
p_{a_{12}} &= 0.966\cdot(\delta s_{a_{x1}} - \delta s_{a_{y2}}) + 0.259\cdot(\delta s_{a_{y1}} - \delta s_{a_{x2}}) \\
p_{a_{13}} &= 0.7071\cdot(\delta s_{a_{x1}} + \delta s_{a_{x3}} - \delta s_{a_{y1}} - \delta s_{a_{y3}}) + [\delta a_x - \delta a_y]\cdot Dt \\
p_{a_{14}} &= 0.966\cdot(\delta s_{a_{x4}} - \delta s_{a_{y1}}) + 0.259\cdot(\delta s_{a_{y4}} - \delta s_{a_{x1}}) \\
&\quad - 0.7071\cdot[(\delta a_z + \delta a_y]\cdot Dt
\end{aligned}
$$

$$p_{a_{23}} = 0.966\cdot(\delta s_{a_{x2}} - \delta s_{a_{y3}}) + 0.259\cdot(\delta s_{a_{y2}} - \delta s_{a_{x3}}) + 0.7071\cdot[(\delta a_z - \delta a_y]\cdot Dt$$

$$p_{a_{24}} = 0.7071\cdot(\delta s_{a_{x2}} + \delta s_{a_{x4}} - \delta s_{a_{y2}} - \delta s_{a_{y4}}) - [\delta a_x + \delta a_y]\cdot Dt$$

$$p_{a_{34}} = 0.966\cdot(\delta s_{a_{x3}} - \delta s_{a_{y4}}) + 0.259\cdot(\delta s_{a_{y3}} - \delta s_{a_{x4}}) \qquad (11)$$

where the $\delta s_{a_{ki}}$ ($k = x,y$; $i = 1,2,3,4$) terms represent total accelerometer error. The separation effect terms, δa_i, appear in the parity equations which have physically separated sensors. $p_{a_{12}}$ and $p_{a_{34}}$ do not contain separation effect terms since these parity equations contain colocated sensors only (see fig. 1). When these parity residuals are compared to a failure threshold to determine if a failure has occurred, the effects of sensor location must be compensated to increase the sensitivity of the failure detection process within acceptable limits.

The development of gyro parity equations and the reduction to sensor errors and separation effects are similar to the accelerometer development. Since the gyros have a larger dynamic range than the accelerometers, however, the compensation of sensor errors and separation effects takes on more importance.

DYNAMIC THRESHOLD GENERATION

Sensor failure detection is determined from a comparison of the parity residuals to a threshold. If the threshold is exceeded, a failure is declared. For the hard-range failures the threshold may be merely a constant. For the mid- and soft-range levels, however, normal dynamic sensor errors and separation effects, which are most pronounced in maneuvers, are larger than sustainable bias errors. For example, during a standard rate turn (3 deg/sec), a gyro scale factor error of 100 ppm yields an equivalent drift rate of 1 deg/hr. A bias level this high would result in serious navigation error.

As suggested by equation (5) and table I, the accelerometer outputs contain static (bias) and dynamic (misalignment and scale factor nonlinearity) errors. Since these errors are statistically known (e.g. from manufacturer's data), an estimate for the maximum first-order accelerometer errors can be written from equation (5) as

$$\delta s_{a_m} = [\lambda_{a_m} + (\varepsilon_{a_m} + \mu_{a_m}) *(|c1*\hat{a}_{x_f}| + |c1*\hat{a}_{y_f}| + |c3*\hat{a}_{z_f}|)]*Dt \qquad (12)$$

where the maximum sensor error terms are determined from table I and equation (1), and the $\hat{a}_{i_f}$ terms are least-squares estimates for accelerations from an appropriate accelerometer pair; also, these terms are filtered to be compatible with the avionics channel under consideration (mid-, or soft-range). An estimate for the maximum accelerometer sensor error contribution to a parity equation is obtained from the coefficients of the dynamic sensor error terms in equation (11) as

$$p_{a_m} = 2.828 * \delta s_{a_m} \tag{13}$$

The constant in equation (13) is the sum of the absolute values of the coefficients of the sensor error terms in parity equations $p_{a_{13}}$, and $p_{a_{24}}$ in equation (12) to account for worst case conditions. The sum of the absolute values of the coefficients in the remaining parity equations is 2.445.

Equation (13) constitutes the compensation for dynamic sensor error to the threshold for failure detection; however, it does not take into account the effects of quantization and sensor noise. The quantization errors in the parity residuals result from the digitization of the sensor torquing loop output for each sensor; the digital pulse weight for the accelerometers is 10^{-3} g at the 64 Hz processing rate. A constant term , T_{aq}, is added to the threshold, therefore, to account for unattenuated quantization and noise. This term constitutes the threshold for the flight control channel. The noise and quantization compensation terms in the filtered channels are determined by the unattenuated residuals.

Two methods have been implemented to provide compensation in the accelerometer thresholds for the separation effects indicated in equation (11) (refs. 4-6). The separation effect terms derived for equation (7) may be obtained from the least-squares solutions of the accelerometer measurements. From equation (3), the estimates for body axis accelerations for IMU1 (accelerometers 1 and 2) are

$$\hat{a}_{x_{12}} = (0.5*(- s_{a_{x1}} + s_{a_{y1}} + s_{a_{x2}} - s_{a_{y2}}))/Dt$$

$$\hat{a}_{y_{12}} = (0.1585*(s_{a_{x1}} - s_{a_{y2}}) + 0.5915*(s_{a_{x2}} - s_{a_{y1}}))/Dt$$

$$\hat{a}_{z_{12}} = (- 0.683*(s_{a_{y1}} + s_{a_{x2}}) - 0.183*(s_{a_{x1}} + s_{a_{y2}}))/Dt$$

and similarly for IMU2,

$$\hat{a}_{x_{34}} = 0.5(s_{a_{x3}} - s_{a_{y3}} - s_{a_{x4}} + s_{a_{y4}})/Dt$$

$$\hat{a}_{y_{34}} = (0.1585*(s_{a_{y4}} - s_{a_{x3}}) + 0.5915*(s_{a_{y3}} - s_{a_{x4}}))/Dt$$

$$\hat{a}_{z_{34}} = (-0.183*(s_{a_{x3}} + s_{a_{y4}}) - 0.683*(s_{a_{y3}} + s_{a_{x4}}))/Dt \qquad (15)$$

These least-squares estimates for acceleration may be used to provide exact compensation for the separation effect terms which appear in the parity residuals given in equation (11). The threshold expressions for each parity equation are,

$$T_{a_{12}} = T_{aq} + 2.445*\delta s_{a_m}$$

$$T_{a_{13}} = T_{aq} + 2.828*\delta s_{a_m} + 1/\sqrt{2}*(|\hat{a}_{x_{34}} - \hat{a}_{x_{12}}| - |\hat{a}_{y_{34}} - \hat{a}_{y_{12}}|)_f*Dt$$

$$T_{a_{14}} = T_{aq} + 2.445*\delta s_{a_m} - 1/\sqrt{2}*(|\hat{a}_{y_{34}} - \hat{a}_{y_{12}}| + |\hat{a}_{z_{34}} - \hat{a}_{z_{12}}|)_f*Dt$$

$$T_{a_{23}} = T_{aq} + 2.445*\delta s_{a_m} + 1/\sqrt{2}*(|\hat{a}_{z_{34}} - \hat{a}_{z_{12}}| - |\hat{a}_{y_{34}} - \hat{a}_{y_{12}}|)_f*Dt$$

$$T_{a_{24}} = T_{aq} + 2.828*\delta s_{a_m} - 1/\sqrt{2}*(|\hat{a}_{x_{34}} - \hat{a}_{x_{12}}| + |\hat{a}_{y_{34}} - \hat{a}_{y_{12}}|)_f*Dt$$

$$T_{a_{34}} = T_{aq} + 2.445*\delta s_{a_m} \qquad (16)$$

where the separation effect terms are appropriately filtered. It is easily seen, however, that false alarms are possible with this method of compensation. That is, a failure in sensor 3 would affect the threshold term for sensors 1 and 4, etc. To correct this deficiency, the method of threshold compensation illustrated in figure 4 was developed.

The parity residuals contain undesirable high frequency terms (compared to vehicle dynamics), which include differential vibration and structural modes, and high frequency electronic noise spikes. Passing the parity residuals through a high pass filter drives low frequency terms, such as lever-arm acceleration and biases toward zero, while compensating the threshold for the high frequency effects which appear in the residuals. This threshold compensation, which is used only in the mid- and soft-range channels tends to render the failure detection process false-alarm free. High frequency lever-arm acceleration effects are compensated in the threshold. The compensation for low frequency components of lever-arm acceleration, however, must be determined separately.

As illustrated in figure 4, the low frequency components of lever-arm acceleration are computed in real time and added directly to each threshold. The required differential separation effects may be computed directly from

equations (6), (7), and (11), and added to equation (16). In $p_{a_{13}}$, for example, the low frequency part of $(\delta a_x - \delta a_y)$ can be formed and added to the total threshold for that parity equation.

$$T_{a_{la}} = (\delta a_x - \delta a_y)$$

$$T_{a_{la}} = [-(\hat{\omega}_y^2 + \hat{\omega}_z^2)\cdot(l_{x2} - l_{x1}) + (\hat{\omega}_y\cdot\hat{\omega}_x - \dot{\hat{\omega}}_z)\cdot(l_{y2} - l_{y1})$$

$$+ (\dot{\hat{\omega}}_y + \hat{\omega}_x\hat{\omega}_z)\cdot(l_{z2} - l_{z1})]\cdot Dt - [(\dot{\hat{\omega}}_z + \hat{\omega}_x\cdot\hat{\omega}_y)\cdot(l_{x2} - l_{x1})$$

$$- (\hat{\omega}_x^2 + \hat{\omega}_z^2)\cdot(l_{y2} - l_{y1}) + (\hat{\omega}_z\cdot\hat{\omega}_y - \dot{\hat{\omega}}_x)\cdot(l_{z2} - l_{z1})]\cdot Dt \qquad (17)$$

This expression is computed directly from gyro measurements converted to body angular rates through least-squares solutions. The angular accelerations are obtained by back differencing the angular rate solutions. Each rate is filtered to be consistent with accelerometer FDI. The absolute value of this expression is added to the threshold.

To summarize, the threshold terms for the vector-based method of accelerometer FDI consist of: 1) a constant to account for quantization and noise; 2) compensation for statistically known terms such as scale factor and misalignment uncompensated errors; 3) a high pass filter to include high frequency residuals in the threshold; and 4) low frequency compensation for lever-arm acceleration.

The gyro threshold function is determined in the same manner as the accelerometer threshold function, except that there is no low frequency compensation to be determined separately (e.g. lever-arm acceleration).

Failure Isolation

Each parity equation is tested against its corresponding threshold, so that, if $(|p_{a_{ij}}| - |T_{a_{ij}}|) > 0$, the parity equation indicates a failure; a logical flag, L_{ij}, is set true for this event. At the completion of all six threshold tests for the parity equations a set of logical equations is examined to isolate a failed instrument. The logical equations are,

$$A_1 = L_{12}\cdot L_{13} + L_{12}\cdot L_{14} + L_{13}\cdot L_{14}$$

$$A_2 = L_{12}\cdot L_{23} + L_{23}\cdot L_{24} + L_{12}\cdot L_{24}$$

$$A_3 = L_{13}\cdot L_{23} + L_{13}\cdot L_{34} + L_{23}\cdot L_{34}$$

$$A_4 = L_{14} \cdot L_{24} + L_{14} \cdot L_{34} + L_{24} \cdot L_{34} \tag{18}$$

where · denotes logical "and" function and + denotes logical "or" function. If sensor 1 fails, L_{12}, L_{13}, and L_{14} will be set true when the parity residuals fail their respective threshold tests. According to equation (18), A_i will be set true (e.g. isolated as failed) when any two flags relative to the same sensor are set true. When A_i is set true, redundancy management removes the entire sensor from further processing even if only one measurement axis fails.

To isolate a second failure only three tests are available. For example, if sensor 1 has failed,

$$A_2 = L_{23} \cdot L_{24}$$

$$A_3 = L_{23} \cdot L_{34}$$

$$A_4 = L_{24} \cdot L_{34} \tag{19}$$

this expression isolates a second failure after sensor 1 has failed. A third failure may be detected but not isolated.

Equations (18) and (19) are applicable to multiple nonconcurrent failures for the gyros or accelerometers. Modifications in the isolation logic are easily implemented to account for the possibility of multiple concurrent failures.

Failure Coverage

A characteristic of TDOF instruments is that a failure may be reflected in either of its measurement axes; also, if a failure occurs in one of the sensitive axes, the second axis is likely to follow. Thus, a failure, which is detected and isolated, results in removal of both axes of the sensor as the logic of equations (18) and (19) indicate.

Because the sensor clusters for the accelerometers and the gyros are symmetric, the first failure is uniformly detectable. That is, if the measurement axes of the instruments were extended in space, the axes would lie uniformly on the surface of a cone; this can also be determined from table II and equations (10) and (11). The first failure for any of the sensors is equally likely to be detected since the parity equation coefficient terms are the same for each sensor axis in the system of equations as given in table II. Once the first failure has been detected and isolated, however, an unsymmetric array of sensors remains. Failures are not equally likely to be detected. From table II it can be seen that it is possible to require a failure level to be 1/0.2588 times the threshold level to detect a failure depending on the sensor under consideration.

It is clear in the system of parity equations of equation (11) that there are sensor failures for which the parity equations are transparent. If both axes of accelerometer 1 open (e.g. null output) simultaneously, $p_{a_{13}}$ would be transparent to the failure; however, $p_{a_{12}}$, and $p_{a_{14}}$ would readily detect the open. On the first failure level, therefore, the accelerometer null would be immediately detected and isolated. On the second failure level, however, the null failure detection and isolation would be delayed, because of the transparency in $p_{a_{13}}$ (or $p_{a_{24}}$) until vehicle dynamics increase the parity residuals to allow failure detection. The same comments apply to third level failure detection if opposite sensors remain after two failures. An analysis of these singularities is given in reference 8.

DESCRIPTION OF SIMULATION

The vector-based failure detection and isolation algorithm for the RSDIMU under consideration was tested with the use of a digital simulation of a commercial transport vehicle (ref. 9). The aircraft is modeled in six degrees of freedom with nonlinear aerodynamics. A flight control system and turbulence is included in the simulation; however, structural modes and vibration have not been included in the vehicle modeling. The skewed gyro and accelerometer arrays are modeled 22 ft. forward of the aircraft cg and separated 4 ft. in both the x and z directions so that the effects of lever-arm acceleration may be assessed. The sensor data is determined from the aircraft equations of motion and input to the FDI algorithms for gyros and accelerometers.

Figure 6 shows the ground track profile used to evaluate the fault tolerant algorithm during the dynamic phases of the vehicle flight. The profile includes features from a commercial transport flying into a microwave landing system environment. The aircraft performs two left turns and four right turns at a constant altitude of 6700 feet at 150 knots before descending at 3000 seconds to 1000 feet to perform a runway alignment maneuver. The aircraft speed at final approach to landing is 130 knots. The aircraft performs decrab and flare maneuvers just before the landing, which occurs at 3409 seconds. The aircraft linear accelerations and angular rates are shown in figures 7 and 8, respectively, to show the magnitude of these quantities as well as to show the accuracy of the RSDIMU least-squares solutions. For the case shown the nominal gust intensity is 6 ft/sec; the wind has a steady state velocity of 10 ft/sec at an angle of 20/. The wind components are shown in figure 9. The three gust conditions considered for this study were 2 ft/sec (light turbulence), 6 ft/sec (moderate turbulence), and 21 ft/sec (extreme turbulence). The ability of the vector-based FDI algorithm to detect failures under turbulent conditions is critical.

The plotting points for the figures were saved at 1-second intervals. For this paper only one complete FDI channel for the RSDIMU was implemented.

DISCUSSION OF RESULTS

This section discusses the results obtained with the simulation just described for the vector-based FDI algorithm. The time histories of the parity residuals and failure detection thresholds are presented using the equations developed in this report. The parity residuals for the gyros and accelerometers, and their respective thresholds are plotted in deg/hr, and g's, respectively.

Figure 10 shows the gyro parity equation residuals obtained, using the equivalent of equation (11) for gyros, for the flight described in figures 6-9. The absolute value of each parity equation residual is shown, since it is this quantity which is measured against a threshold for failure detection. The unfiltered residuals are random in nature because of sensor quantization; also, the effects of maneuvers in the last half of the flight are barely evident. The quantization pulses evident in residuals $p_{g_{13h}}$, and $p_{g_{24h}}$ are the result of the symmetry in the parity equation coefficients. The peak value of the residuals is about 196 deg/hr. The mid-range parity equation residuals are passed through a first-order low-pass filter with time constant of 10 seconds. The effects of dynamics are plainly evident after the unaccelerated portion of the flight. The peak value in $P_{g_{24m}}$ is 2.43 deg/hr. The soft-range parity residuals are passed through a first-order low-pass filter with time constant of 30 seconds. The peak residual during the landing maneuver is 1.47 deg/hr.

From figure 10 it is apparent that the effects of vehicle maneuvers warrants the use of dynamic failure detection thresholds. If a constant threshold were used it would have to be large enough to accommodate all the possible maneuvers the aircraft would experience. This would compromise the ability of the system to detect failures during unaccelerated portions of the flight, and hence the performance of the navigation outputs. Therefore, the use of dynamic thresholds which are sensitive to dynamics is justified.

Figure 11 shows the hard- and soft-range accelerometer parity residuals for the same flight. As in the case of the gyro parity residuals, the absolute values are shown. The hard-failure channel residual is random in nature because of quantization and is relatively unaffected by vehicle maneuvers. The soft-accelerometer channel residuals appear to be relatively unaffected during this flight; however, this is caused in part by the high noise level created by the turbulent environment. The low-pass filter time constant for the soft channel residual is 5 seconds. The peak values for the hard- and soft-range parity residuals are 4.44×10^{-3} g and 2.56×10^{-4} g, respectively. The quantization effects apparent in the residuals for $p_{a_{13h}}$, and $p_{a_{24h}}$, are the result of the symmetry in the parity equation coefficients. Because of the limited dynamic range of the accelerometers there was no mid-range accelerometer FDI channel implemented for this paper.

The threshold levels obtained for the vector-based FDI algorithm are given in table III. The values used for uncompensated errors are given in table I. Since equation (13) represents a worst case situation for

threshold generation, 2-σ values were used for the uncompensated errors given in table I. This renders a minimum detectable first failure for the soft gyro channel of 0.19 deg/hr and 1.5×10^{-3} g for the soft accelerometer channel. The mid-range gyro threshold constant, and the hard-range gyro and accelerometer channels are design values and are arbitrarily set for this paper. The gyro and accelerometer low frequency dynamic threshold functions as given by equation (17), exclusive of the separation effect terms, are shown in figure 12. These thresholds clearly indicate the need for dynamic threshold compensation during the maneuvering portion of the flight. They also indicate the failure sensitivity during the constant portion of the flight and the importance of maintaining minimum time constants in the soft- and mid-range failure detection channels to maintain that sensitivity. The dynamic threshold in the case of the soft gyro channel is more than an order of magnitude greater during maneuvers than in constant and level flight. The normal scale factor and misalignment error at 3 deg/s is 3.4 deg/hr.

The dynamic portion of the threshold given in figure 12 compensates for low frequency dynamic errors. Unattenuated high frequency noise is compensated through the washout filter as shown in figure 4 while constant biases and low frequency terms are driven toward zero. The effects of these terms are given in figure 13 for the soft gyro channel. The time constant for the washout filter is a design parameter and is set to 150 seconds for this paper.

As indicated in figure 5, each set of parity residuals for the gyro and accelerometer channels (soft-, mid-, and hard-) are subjected to threshold tests to determine if a failure has occurred. The results of the threshold test for the soft gyro and accelerometer channels is given in figures 14 and 15. A positive result for the threshold test would indicate a failure detection. The sensitivity for failure detection is greatest during the unaccelerated portion of the flight as indicated in both figures. The results of the threshold test are always well behaved; therefore, this indicates the propensity toward false alarms is low. The effects of maneuvers is to drive the results of the test more negative; this is reasonable since the sensor errors are greatest during maneuvers.

Sensor failures were introduced into the simulated aircraft system to test the FDI capability of the vector-based algorithm. The injected failures were intended to cover the spectrum of failures for all the channels of operation. The failures were repeated for three levels of wind disturbance, light, moderate, and extreme. The results are listed in table IV. The first two flights covered the ground track given in figure 6. In each of these flights three failures were inserted in the gyro signals at the times indicated in the table. In the first flight the 25 deg/hr failure was detected in a timely fashion for all the turbulence environments. The open failure took six cycles to detect in light turbulence; two cycles in moderate turbulence; and it was detected on cycle in the extreme turbulence case. The hard failure was detected on cycle in all three environments.

The accelerometer failures for the first flight included a soft first failure and a null second failure. The first failure was detected in a timely fashion in the soft channel, but the null failure took 20, 34, and 8 seconds to detect for the light, medium, and extreme levels of turbulence,

respectively. This delay is caused by the transparency in parity equation $p_{a_{24}}$ to null type failures as previously discussed.

For the second flight, two soft failures were injected in the gyro and accelerometer signals and a third hard failure was added to the gyro. The soft gyro failures were not detected in the extreme turbulence environment. The gyro hard failure was detected on cycle. The accelerometer failures were detected in a timely fashion.

The third and fourth flights included only the final 1800 seconds of the flight path given in figure 6. As indicated in table IV, three soft-level failures were added to the gyros and two soft failures were added to the accelerometer signals in flight 3. All failures were detected in a timely fashion.

Three failures were added to the accelerometer signals and two failures to the gyro signals for the fourth flight. Both axes of gyro 1 and accelerometer 1 were failed open at 300 seconds; both failures were detected on cycle. A second soft level failure was added to the gyro and accelerometer axes x2 at 600 seconds. The accelerometer failure was detected and correctly isolated in approximately 90 seconds under all turbulence environments. The gyro failure was only detected and isolated in the light wind turbulence environment.

CONCLUDING REMARKS

A vector based failure detection and isolation algorithm has been developed for a dual fail-operational, separated, and communicating redundant strapdown inertial measurement unit. The performance of the algorithm has been demonstrated via simulation for a broad spectrum of failures in light, moderate, and extreme turbulence environments. The development of failure detection thresholds which are sensitive to low and high frequency disturbances was a major consideration in the development of the algorithm. It is clear that turbulence affects the FDI algorithm capability to detect navigation level gyro failures, while the accelerometer FDI is minimally affected. The gyro and accelerometer FDI functioned without false alarm or incorrect isolation of failure under the conditions presented.

REFERENCES

1. Anon.: Preliminary Design of a Redundant Strapdown Inertial Unit Using Two Degree-of-Freedom Tuned Gimbal Gyroscopes. NASA CR-145035, October 1976.

2. Morrell, Frederick R.; and Russell, J.: Design of a Developmental Dual Fail Operational Redundant Strapdown Inertial Measurement Unit. Proceedings of NAECON '80, Dayton, Ohio, May 1980.

3. Baum, R.; Morrison, E.; and Peters, R.: A Redundant Inertial Navigation System for IUS. AGARD Conference Proceedings No. 272, August 1979.

4. Morrell, Frederick R.; and Motyka, Paul: Unified Analysis Methods for a Fault Tolerant Redundant Strapdown Inertial Measurement Unit. Proceedings of the 5th Digital Avionics Conference, Seattle Washington, November 1983.

5. Bryant, W.H.; Morrell, F.R.; and Bailey, M.L.: Flight Test Configuration for Verifying Inertial Sensor Redundancy Management Techniques. AIAA paper 84-2496, Aircraft Operations and Design Meeting, San Diego, California, November, 1984.

6. Motyka, P.: Fault Detection for Two Physically Separated Communicating Inertial Measurement Units. Proceedings of the Joint Automatic Control Conference, June 1981.

7. Craig, R.J.; and Russell, J.: Failure Modes and Redundancy Analysis for the Multifunction Inertial Reference Assembly (MIRA). AFFDL: TR-78-25, March, 1978.

8. Ebner, R.E.; and Mark, J.E.: Redundant Integrated Flight Control/Navigation Inertial Sensor Complex. Journal of Guidance and Control, Vol. 1, No. 2, March-April 1978, pp143-179.

9. Halyo, N.: Terminal Area Automatic Navigation, Guidance, and Control Research Using the Microwave Landing System (MLS). NASA CR-3681, April 1983.

APPENDIX

DERIVATION OF PARITY EQUATIONS IN TERMS OF SENSOR ERRORS AND SEPARATION EFFECTS

The derivation for $p_{a_{14}}$ in terms of sensor errors and separation effects is shown as a representative case. Starting with the expression for $p_{a_{14}}$ from equation (10),

$$p_{a_{14}} = 1/\sqrt{2}\cdot(a_1^y - a_4^y + a_1^z - a_4^z)\cdot Dt \tag{A1}$$

the expression for a_i^B is obtained from equation (1).

$$\begin{aligned} a_1^y &= \quad c2\cdot s_{a_{x1}} - c1\cdot s_{a_{y1}} \\ a_4^y &= -\, c1\cdot s_{a_{x4}} + c2\cdot s_{a_{y4}} \\ a_1^z &= -\, c3\cdot s_{a_{x1}} - c3\cdot s_{a_{y1}} \\ a_4^z &= -\, c3\cdot s_{a_{x4}} - c3\cdot s_{a_{y4}} \end{aligned} \tag{A2}$$

Parity equation $p_{a_{14}}$ becomes in terms of sensor measurements,

$$p_{a_{14}} = 1/\sqrt{2}\cdot((c2-c3)\cdot s_{a_{x1}} - (c2-c3)\cdot s_{a_{y4}} + (c3+c1)\cdot s_{a_{x4}} - (c3+c1)\cdot s_{a_{y1}}$$

$$= 0.966\cdot(s_{a_{x4}} - s_{a_{y1}}) + 0.2588\cdot(s_{a_{y4}} - s_{a_{x1}}) \tag{A3}$$

Next, substitute for the sensor measurements using equation 5, taking care to identify the location of the sensors. The expression is

$$p_{a_{14}} = 0.966(\delta s_{a_{x4}} - \delta s_{a_{y1}}) + 0.2588(\delta s_{a_{y4}} - \delta s_{a_{x1}}) + [0.966(-c2 \cdot a_{x2} - c1 \cdot a_{y2} - c3 \cdot a_{z2} - c2 \cdot a_{x1} + c1 \cdot a_{y1} + c3 \cdot a_{z1}) + .2588(c1 \cdot a_{x2} + c2 \cdot a_{y2} - c3 \cdot a_{z2} + c2 \cdot a_{x1} - c2 \cdot a_{y1} + c3 \cdot a_{z1})] \cdot Dt \quad (A4)$$

where a_{x2} and a_{x1} represents the x-axis acceleration at locations IMU2, and IMU1, respectively.

$$p_{a_{14}} = 0.966(\delta s_{a_{x4}} - \delta s_{a_{y1}}) + 0.2588(\delta s_{a_{y4}} - \delta s_{a_{x1}}) + 0.7071(a_{y1} - a_{y2} + a_{z1} - a_{z2}) \cdot Dt \quad (A5)$$

From equation (7) this simplifies to

$$p_{a_{14}} = 0.966(\delta s_{a_{x4}} - \delta s_{a_{y1}}) + 0.2588(\delta s_{a_{y4}} - \delta s_{a_{x1}}) - 0.7071(\delta a_z + \delta a_y) \cdot Dt \quad (A6)$$

which is the same as equation (11).

TABLE I.- TWO DEGREE-OF-FREEDOM GYRO AND ACCELEROMETER PARAMETERS

Error Coefficients	Units	One Sigma Values
Accelerometer fixed bias	g	10^{-4}
Accelerometer misalignment	arc sec	12
Accelerometer scale factor error	ppm	100
Accelerometer random noise	$ft/sec^{3/2}$	0.0025
Accelerometer scale factor	ft/sec/pulse	5×10^{-4}
Gyro non-g sensitive bias	deg/hr	0.015
Gyro g-sensitive bias	deg/hr/g	0.015
Gyro misalignment	arc sec	12
Gyro scale factor error	ppm	100
Gyro scale factor	arc sec/pulse	0.635
Gyro random noise	deg/$\sqrt{hr}$	0.002-0.01

TABLE II.- FAILURE DETECTION SENSITIVITY FOR VECTOR-BASED ALGORITHM

Sensor	Parity Equation Residual					
	$P_{a_{12}}$	$P_{a_{13}}$	$P_{a_{14}}$	$P_{a_{23}}$	$P_{a_{24}}$	$P_{a_{34}}$
$s_{a_{1x}}$	0.96593	0.70711	-0.25882			
$s_{a_{1y}}$	0.25882	-0.70711	-0.96593			
$s_{a_{2x}}$	-0.25882			0.96593	0.70711	
$s_{a_{2y}}$	-0.96593			0.25882	-0.70711	
$s_{a_{3x}}$		0.70711		-0.25882		0.96593
$s_{a_{3y}}$		-0.70711		-0.96593		0.25882
$s_{a_{4x}}$			0.96593		0.70711	-0.25882
$s_{a_{y4}}$			0.25882		-0.70711	-0.96593

TABLE III.- GYRO AND ACCELEROMETER CONSTANT THRESHOLD FACTORS

Sensor	Channel	Threshold
Gyro	Hard	1795 deg/hr
	Mid	4 deg/hr
	Soft	0 deg/hr
Accelerometer	Hard	0.298 g
	Soft	0 g

TABLE IV.- FAILURE DETECTION AND ISOLATION CAPABILITY FOR VECTOR-BASED ALGORITHM

Flt. No.	Failure Magnitude	Sensor Axis Failed	Insertion Time (s)	Isolation Time (s) Turbulence Environment Light	Moderate	Extreme	Channel
			Gyro Failures				
1							
	25 °/hr	x1	900	1.28125	1.625	3.34375	mid
	open	x2,y2	2100	0.09375	0.03125	0.0	mid
	3600 °/hr	x3	3400	0.0	0.0	0.0	hard
2							
	0.2 °/hr	x1	600	262	262	n.d.*	soft
	-0.85 °/hr	x2	2100	21	21	n.d.	soft
	1800 °/hr	x3	3400	0.0	0.0	0.0	hard
3							
	-0.85 °/hr	x2	300	81	80	83	soft
	-0.85 °/hr	y1	600	154	152	154	soft
	0.85 °/hr	x3	900	110	111	124	soft
4							
	open	x1,y1	300	0.03125	0.0	0.0	hard
	0.25 °/hr	x2	600	882	n.d.	n.d.	soft
			Accelerometer Failures				
1							
	1.5×10^{-3} g	x1	900	182	186	213	soft
	open	x2,y2	2100	20	34	8	soft
2							
	2×10^{-3} g	x1	1200	100	102	121	soft
	2×10^{-3} g	x2	2700	213	215	201	soft
3							
	2×10^{-3} g	x1	300	104	103	113	soft
	2×10^{-3} g	x2	600	200	201	208	soft
4							
	open	x1,y1	300	0.0	0.0	0.0	hard
	3×10^{-3} g	x2	600	90	91	90	soft
	2.0 g	x3,y3	2100	0.0	0.0	0.0	hard

* n.d. not detected

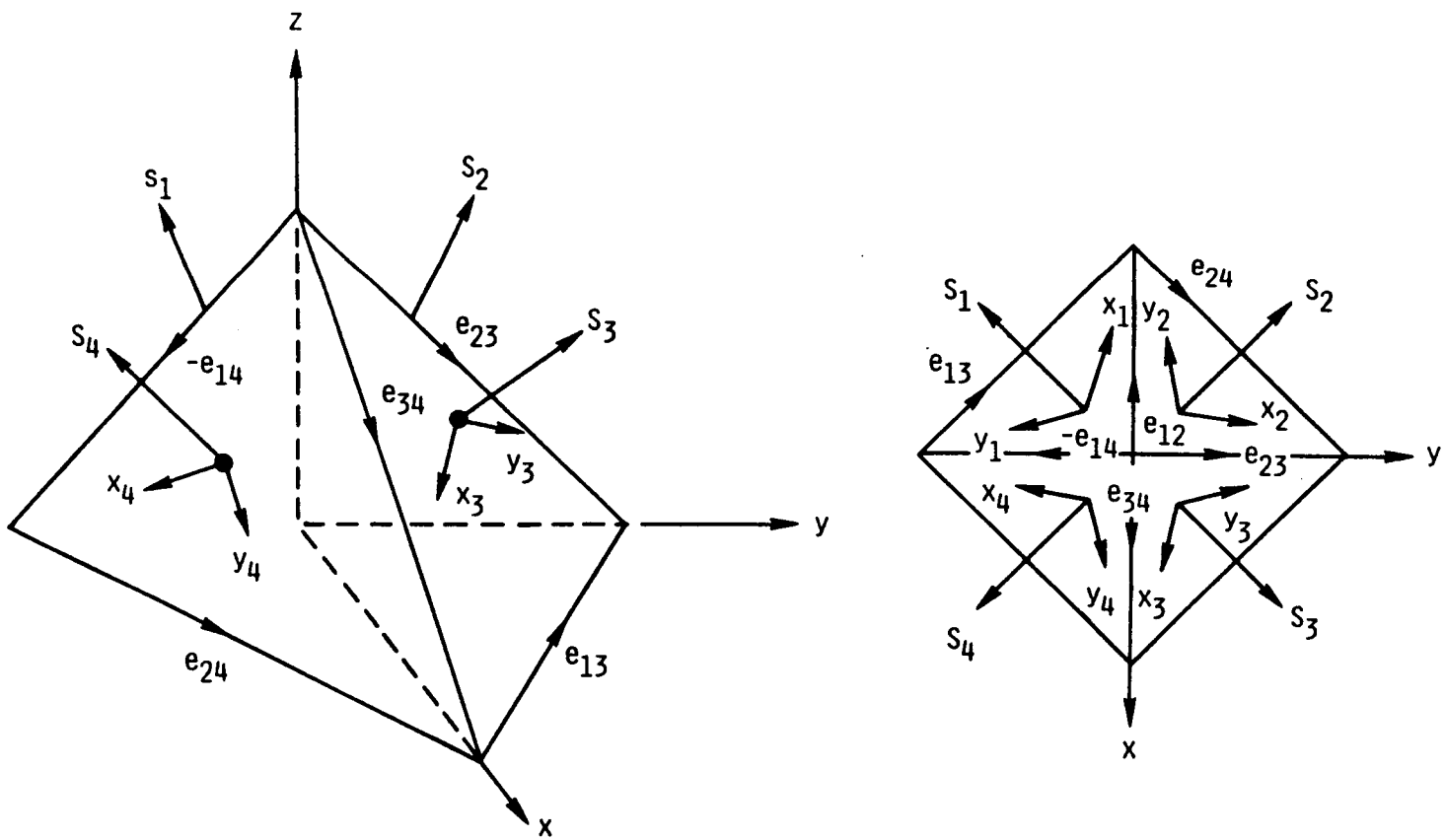

Figure 1. Redundant strapdown inertial measurement unit geometry.

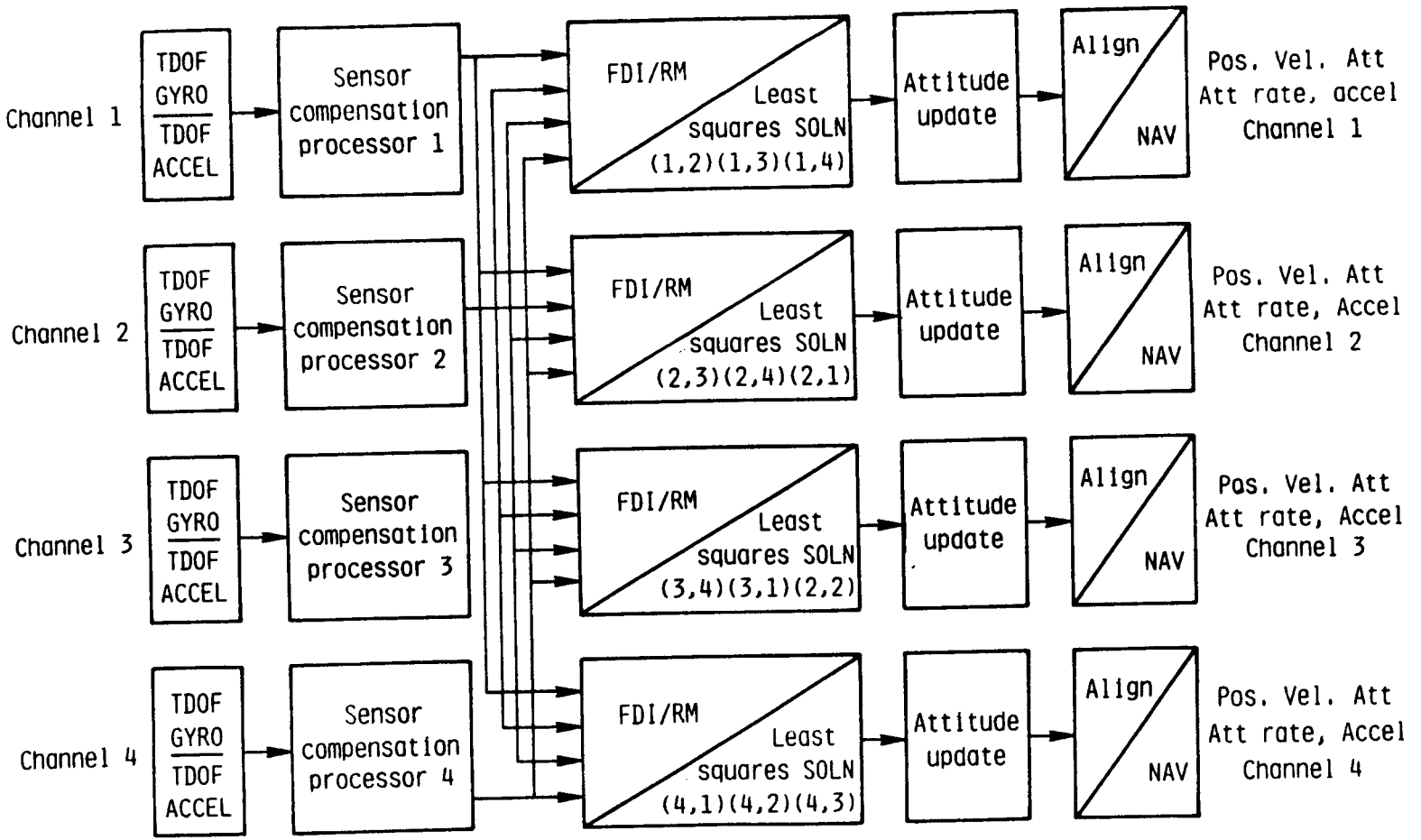

Figure 2. Redundant strapdown inertial measurement unit software data flow.

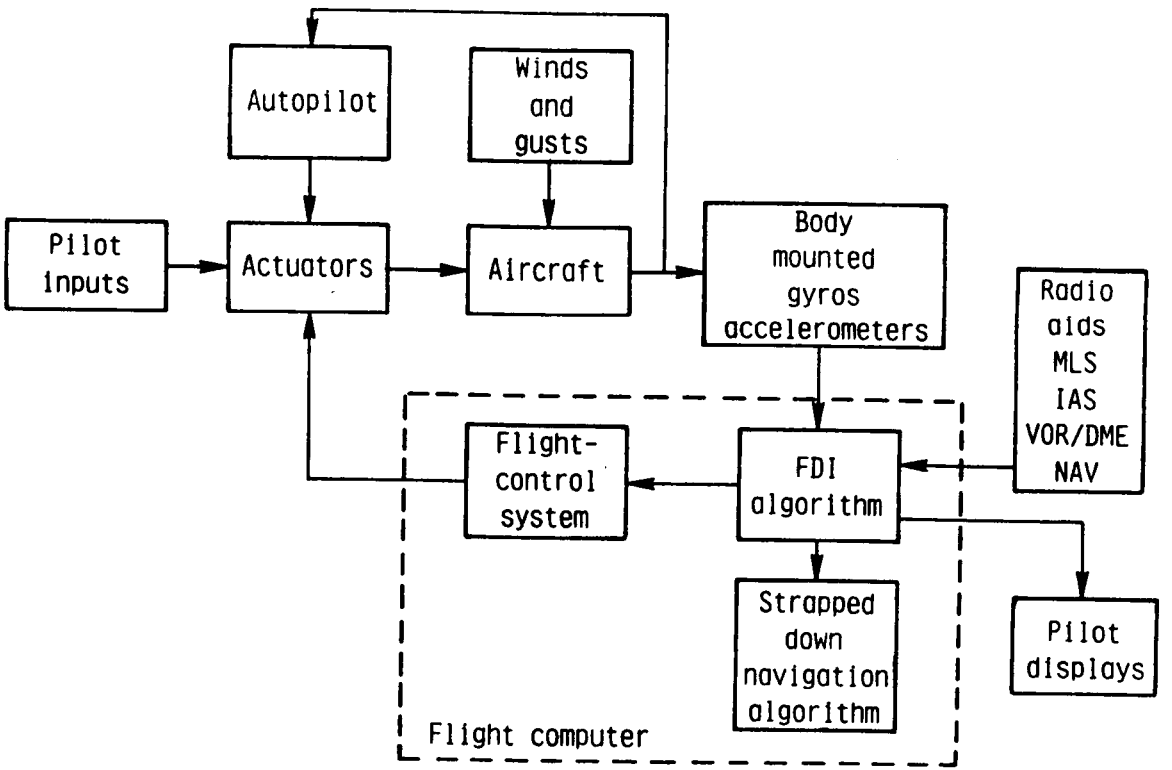

Figure 3. Fault tolerant integrated avionics perspective.

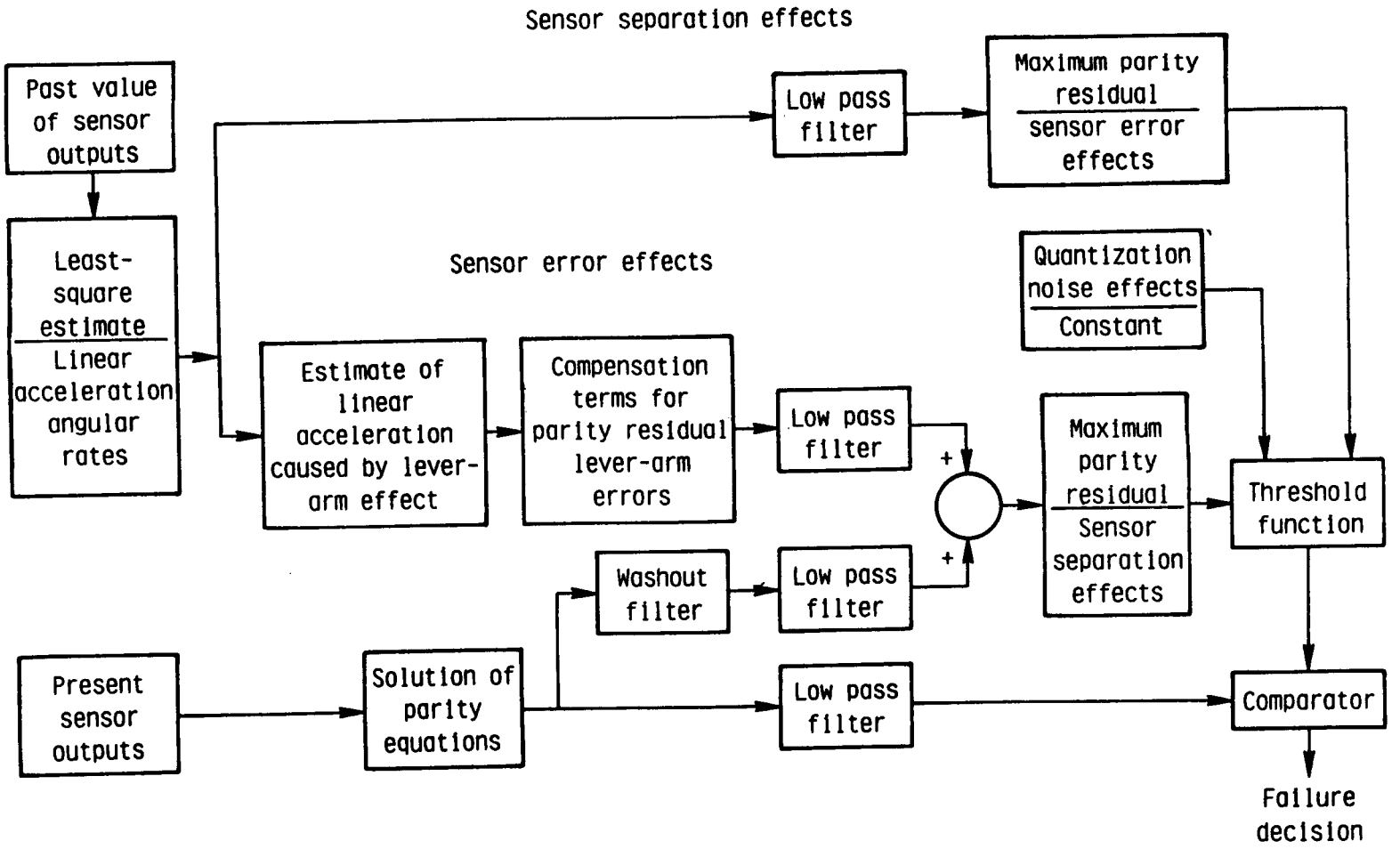

Figure 4. Failure detection and threshold compensation process.

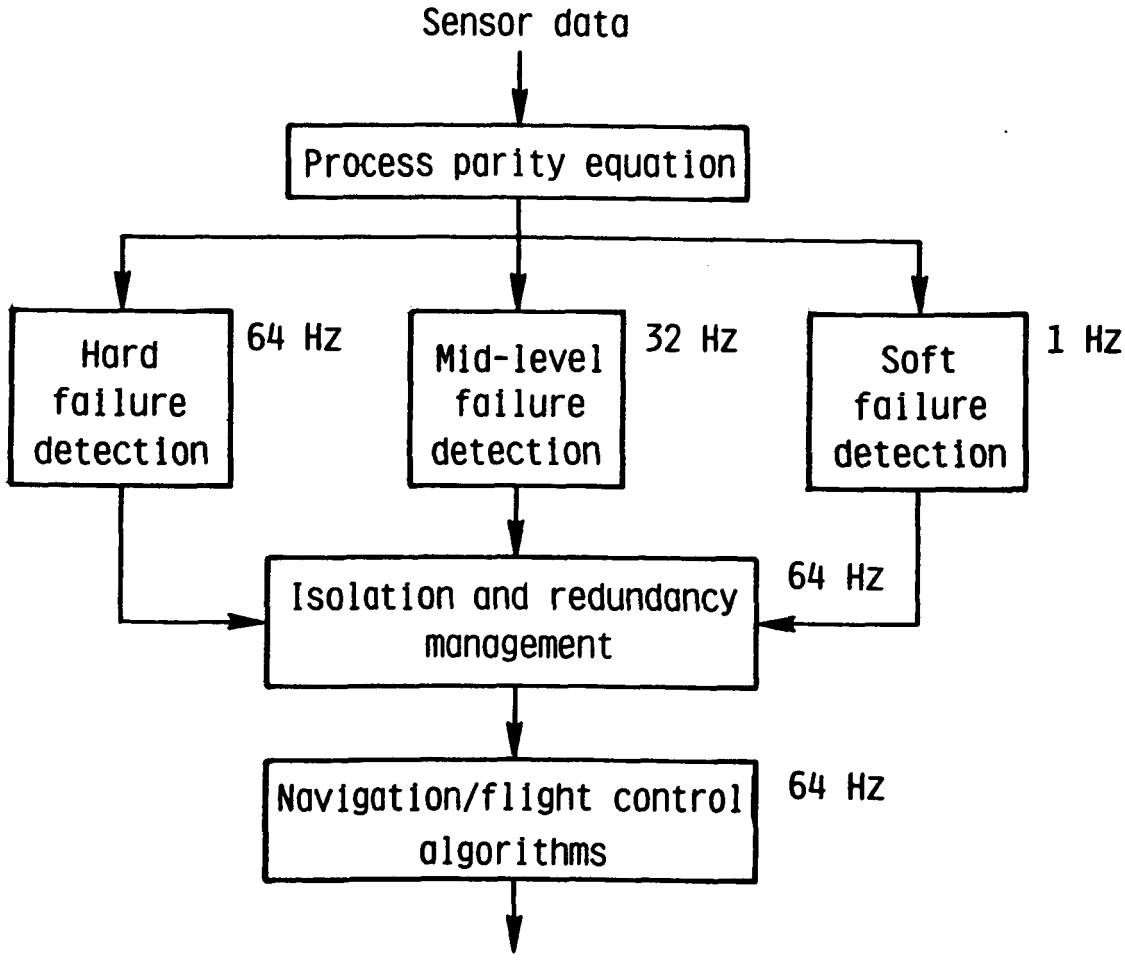

Figure 5. Multi-level structure and FDI processing flow.

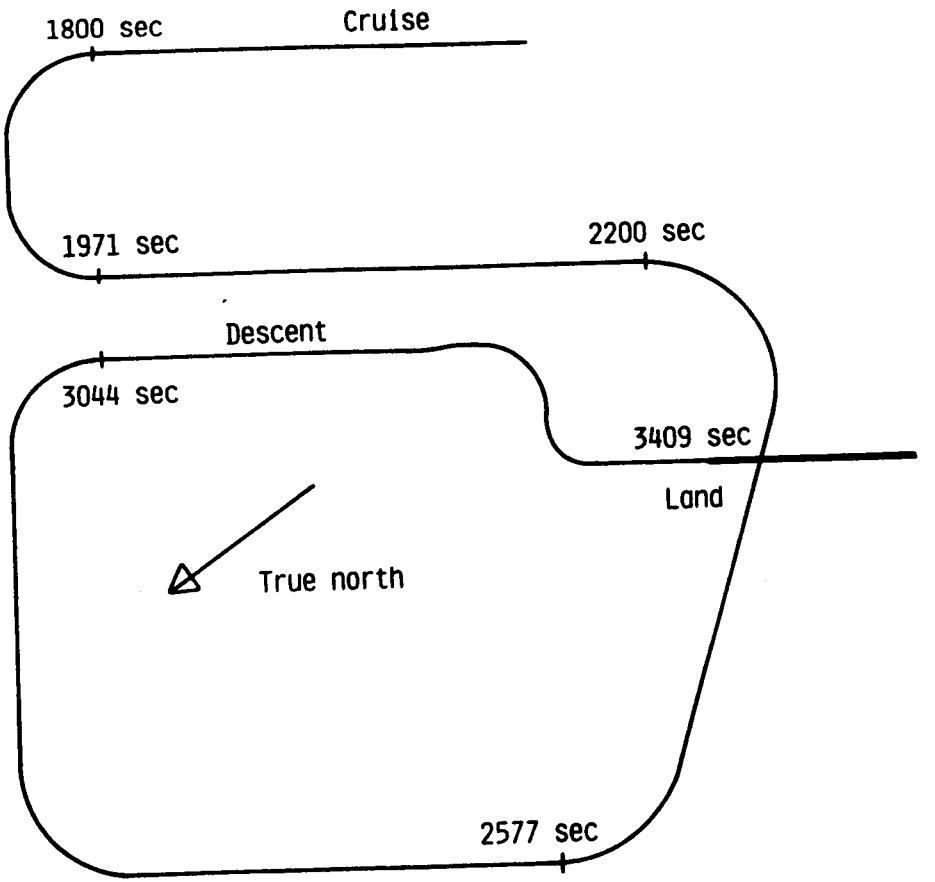

Figure 6. Ground track profile for evaluation of fault tolerant algorithm.

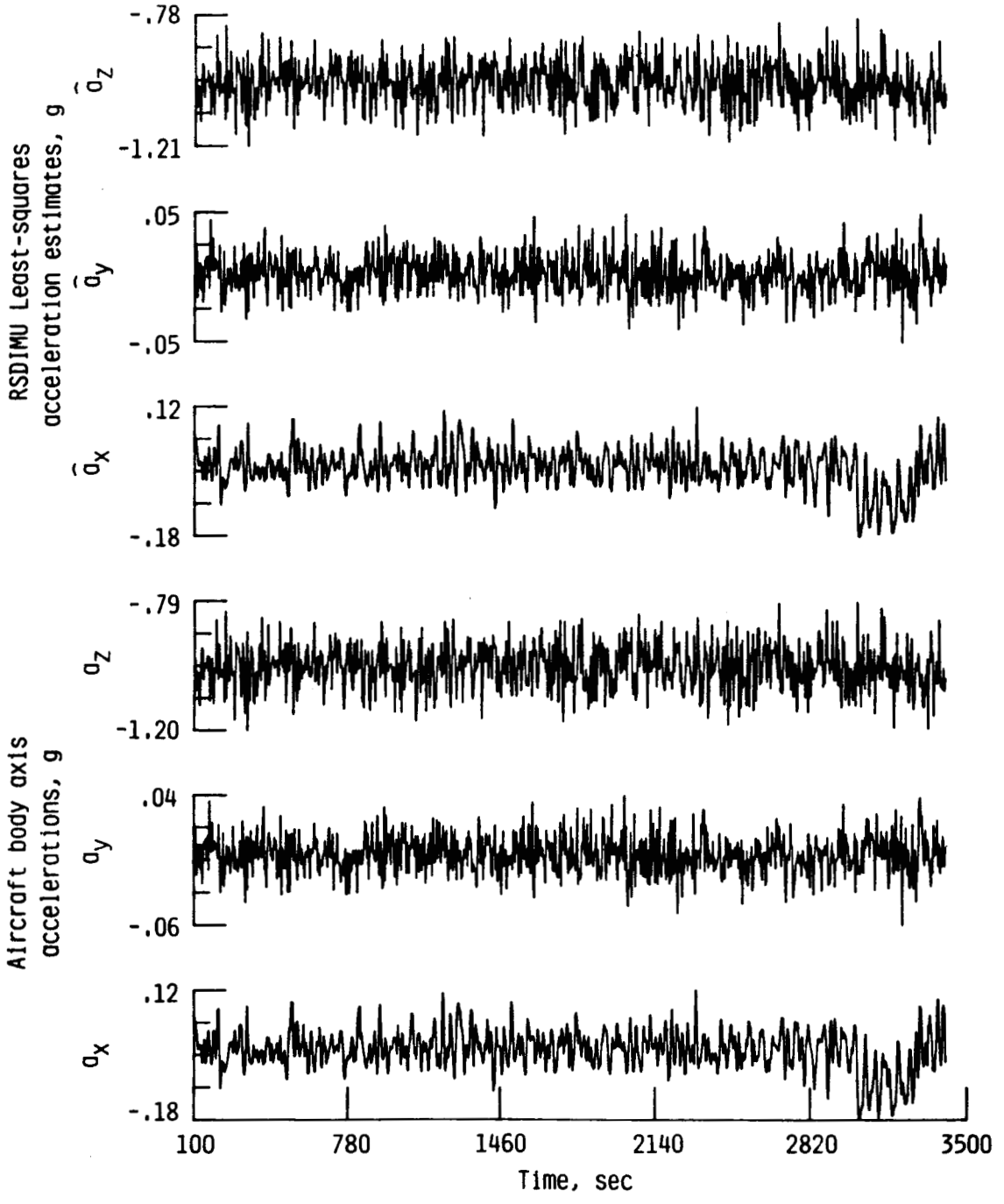

Figure 7. Aircraft accelerations and corresponding IMU least-squares solutions.

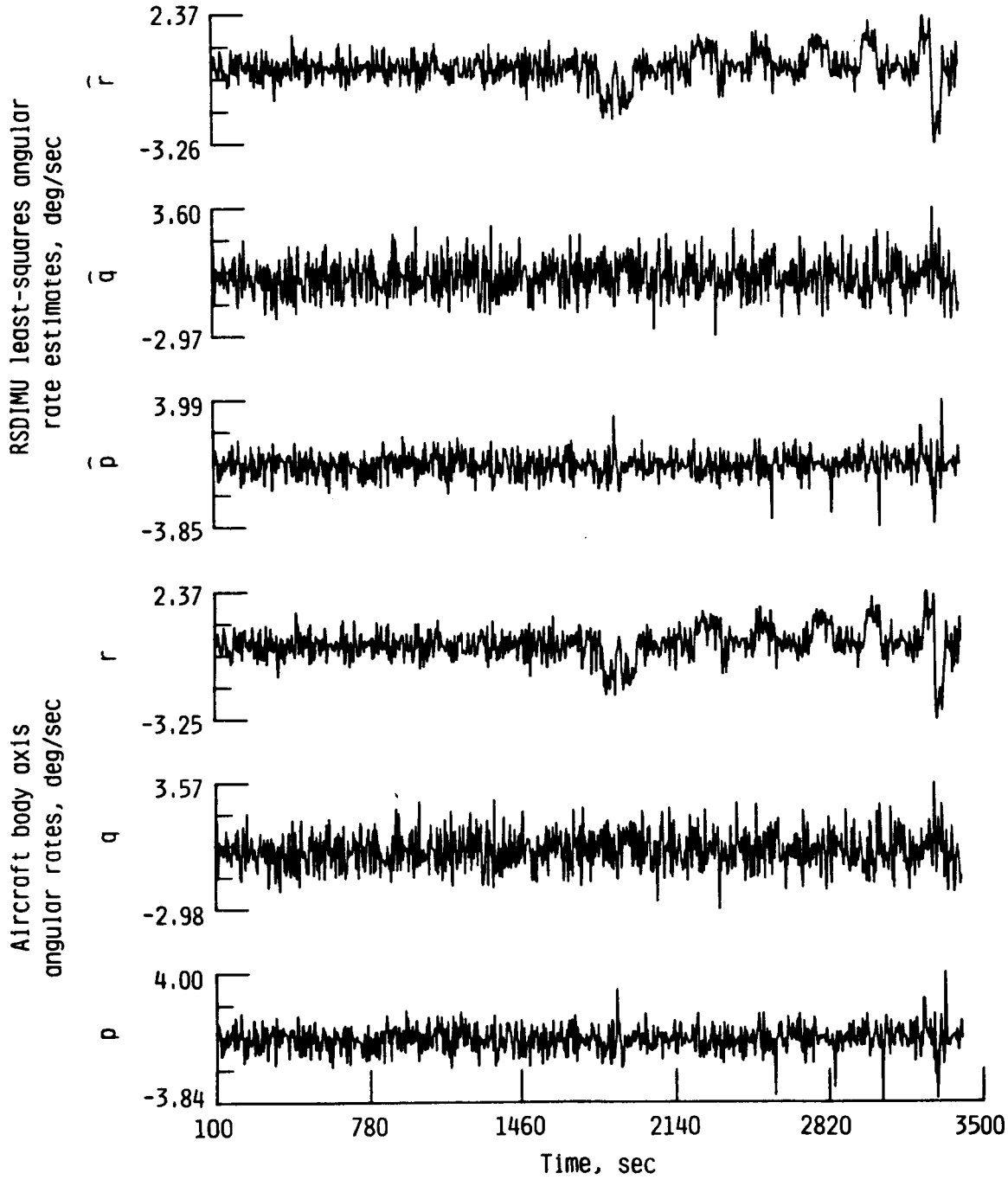

Figure 8. Aircraft angular velocities and corresponding IMU least-squares solutions.

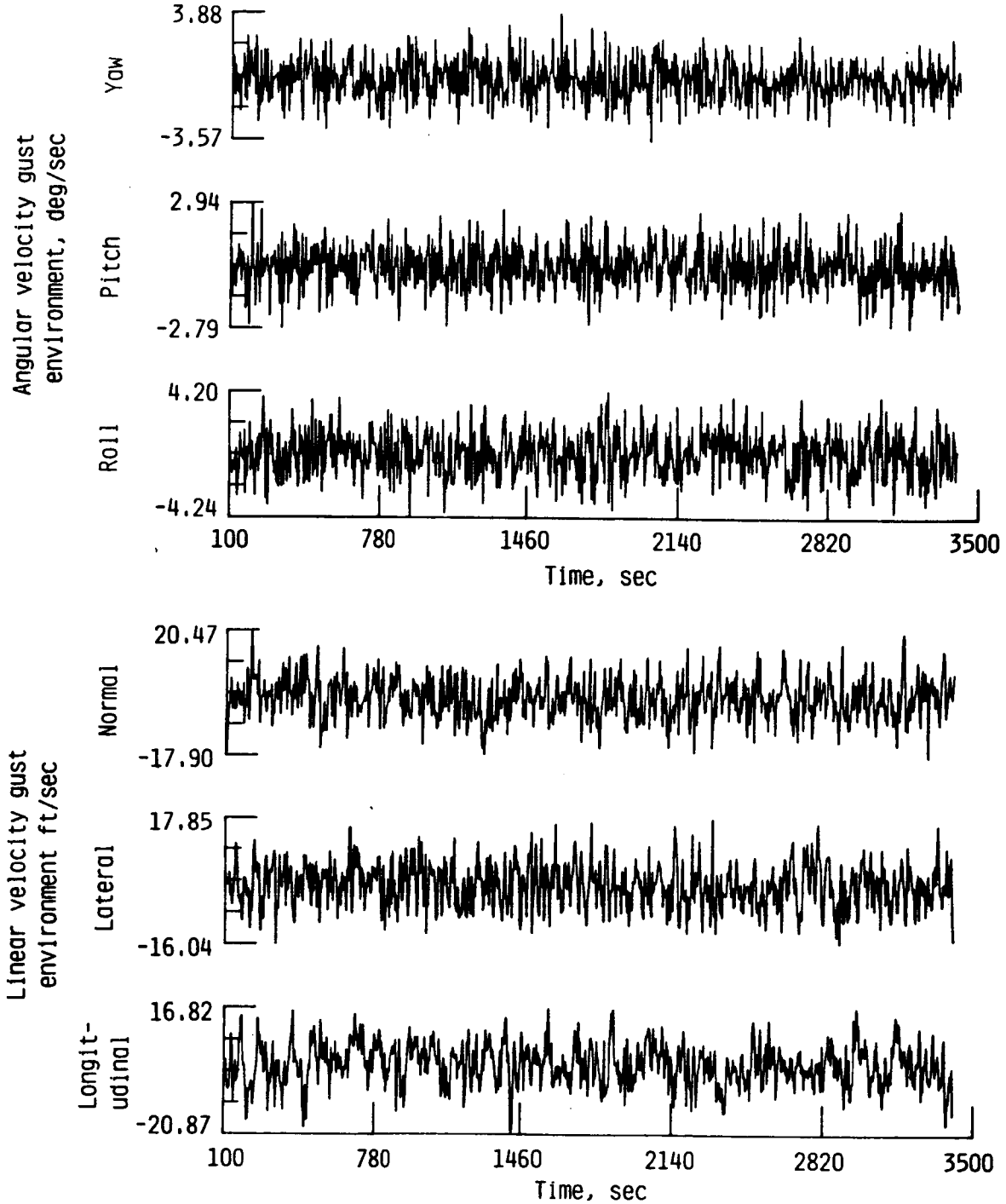

Figure 9. Aircraft gust environment for 6 ft./sec (one sigma) intensity.

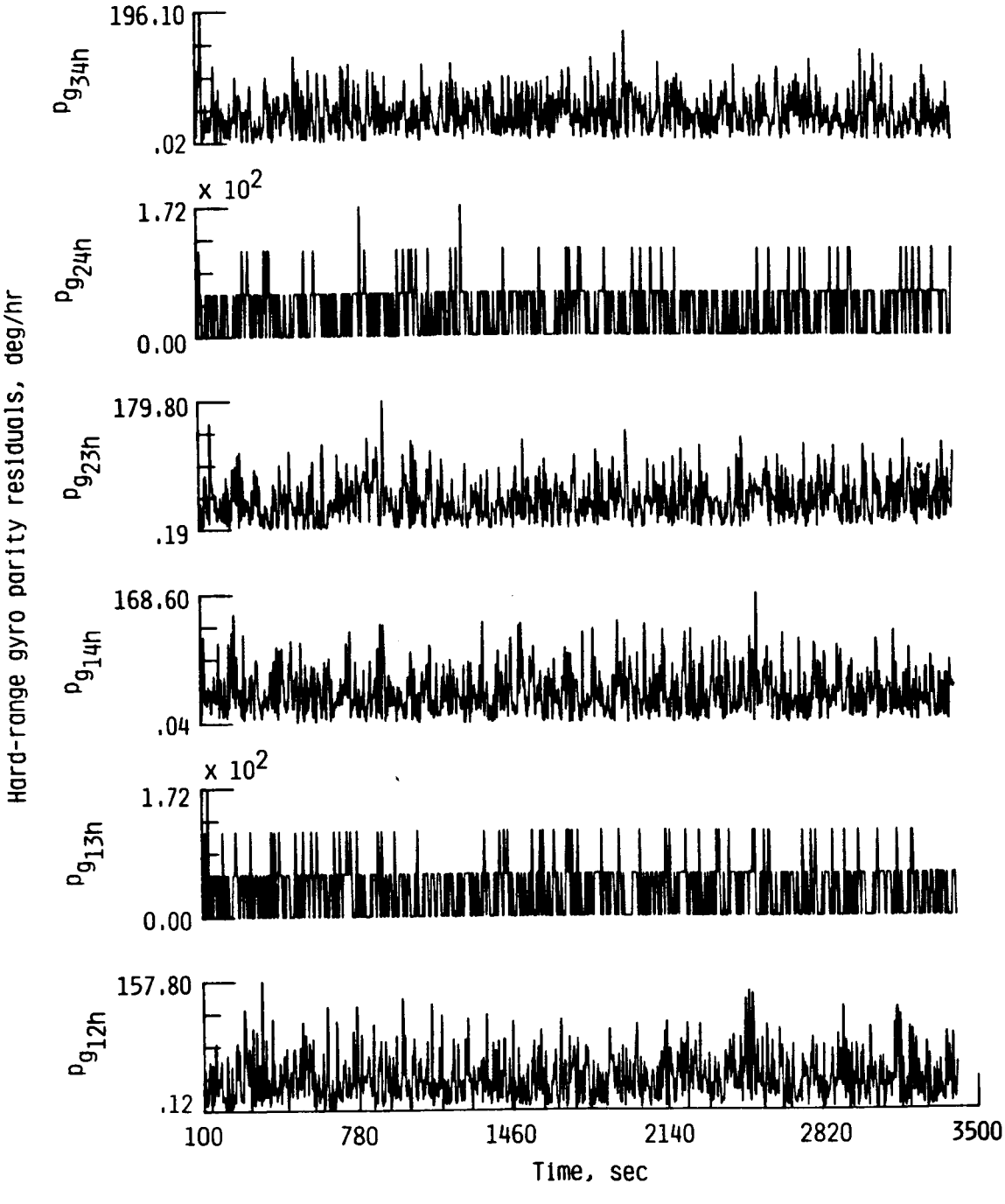

a. Unfiltered gyro parity residuals.

Figure 10. Gyro parity residuals for evaluation trajectory.

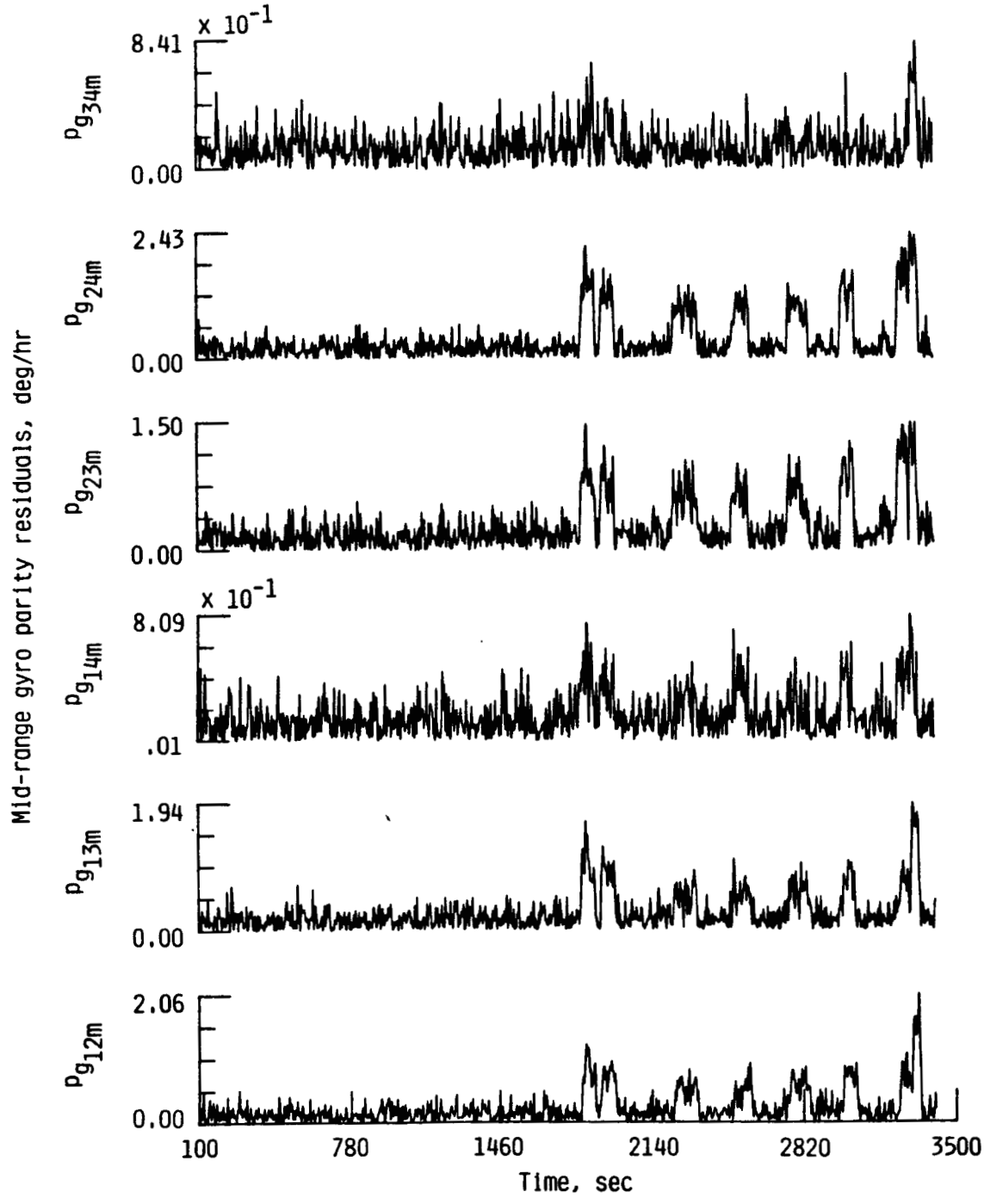

b. Lightly filtered gyro parity residuals.

Figure 10. Continued.

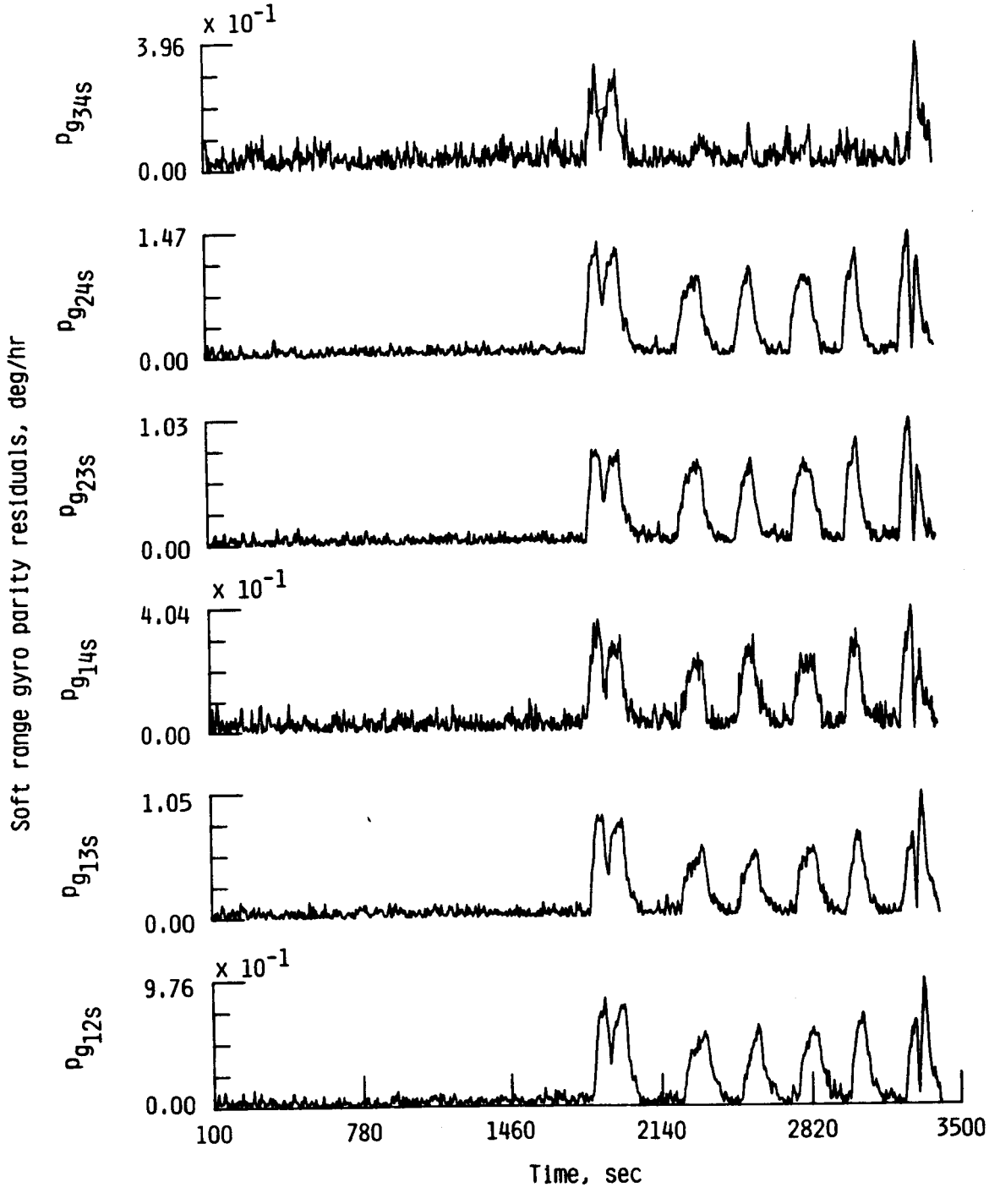

c. Heavily filtered gyro parity residuals.

Figure 10. Concluded.

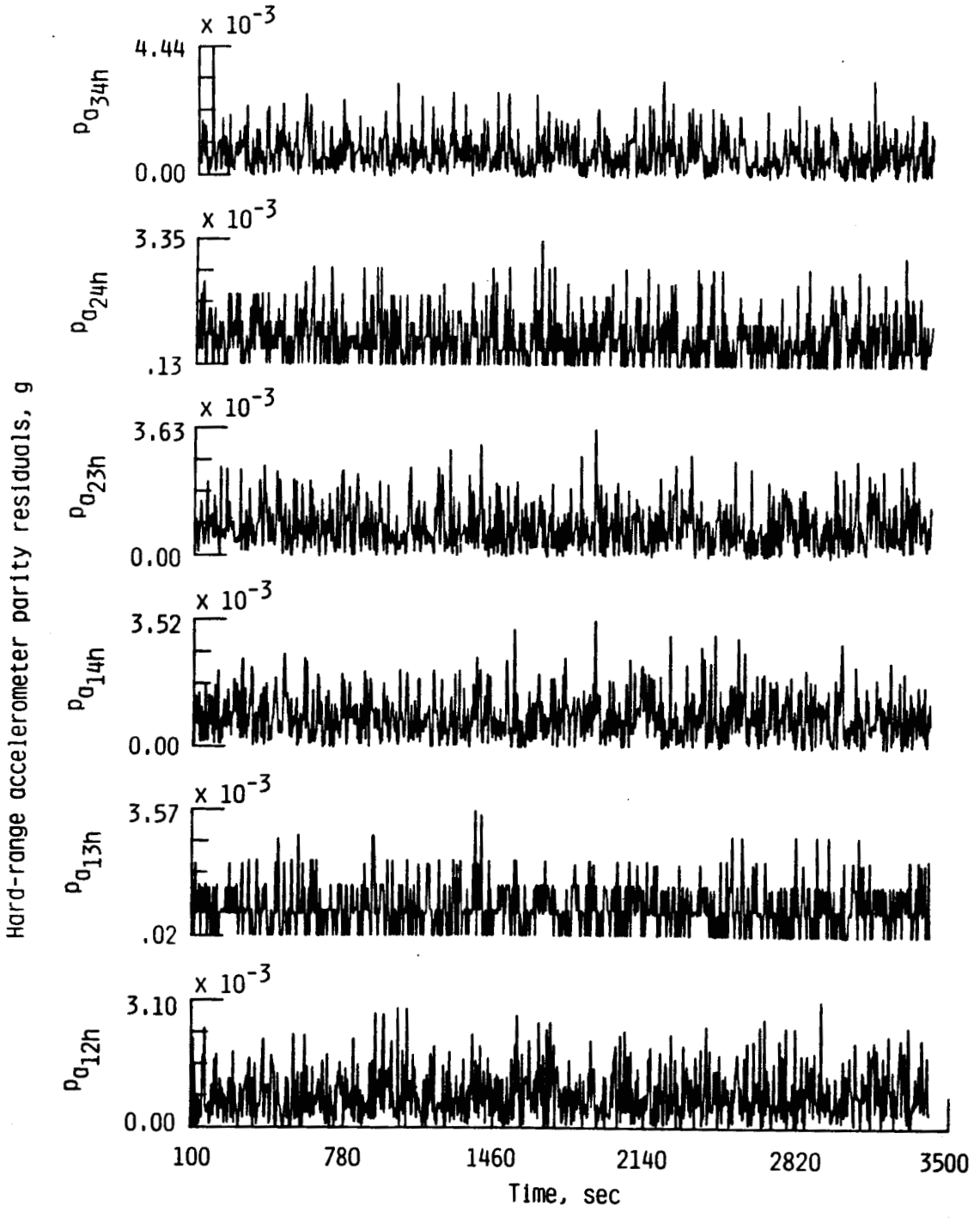

a. Unfiltered hard-channel residuals.

Figure 11. Accelerometer parity residuals for evaluation trajectory.

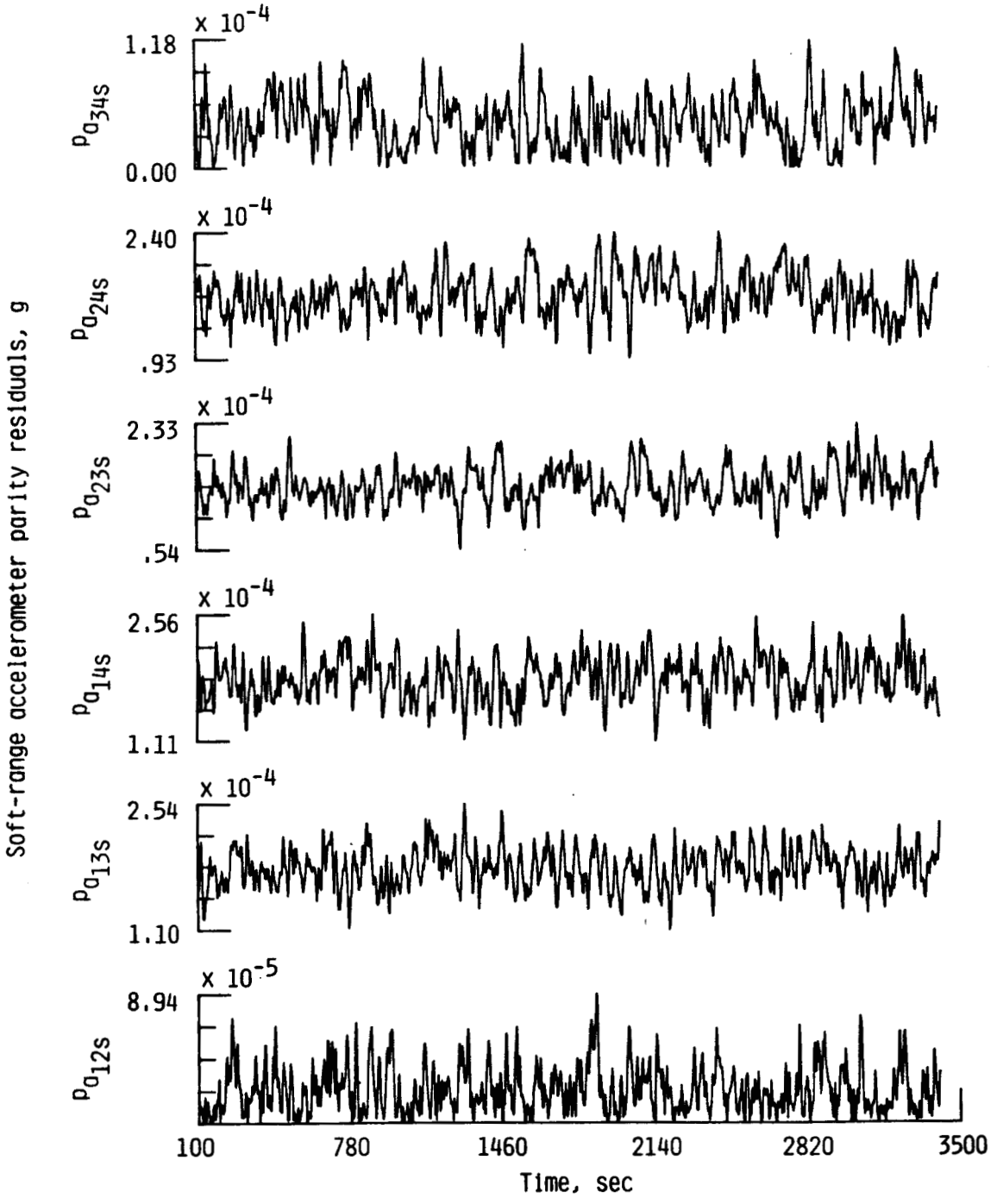

b. Filtered soft-channel residuals.

Figure 11. Concluded.

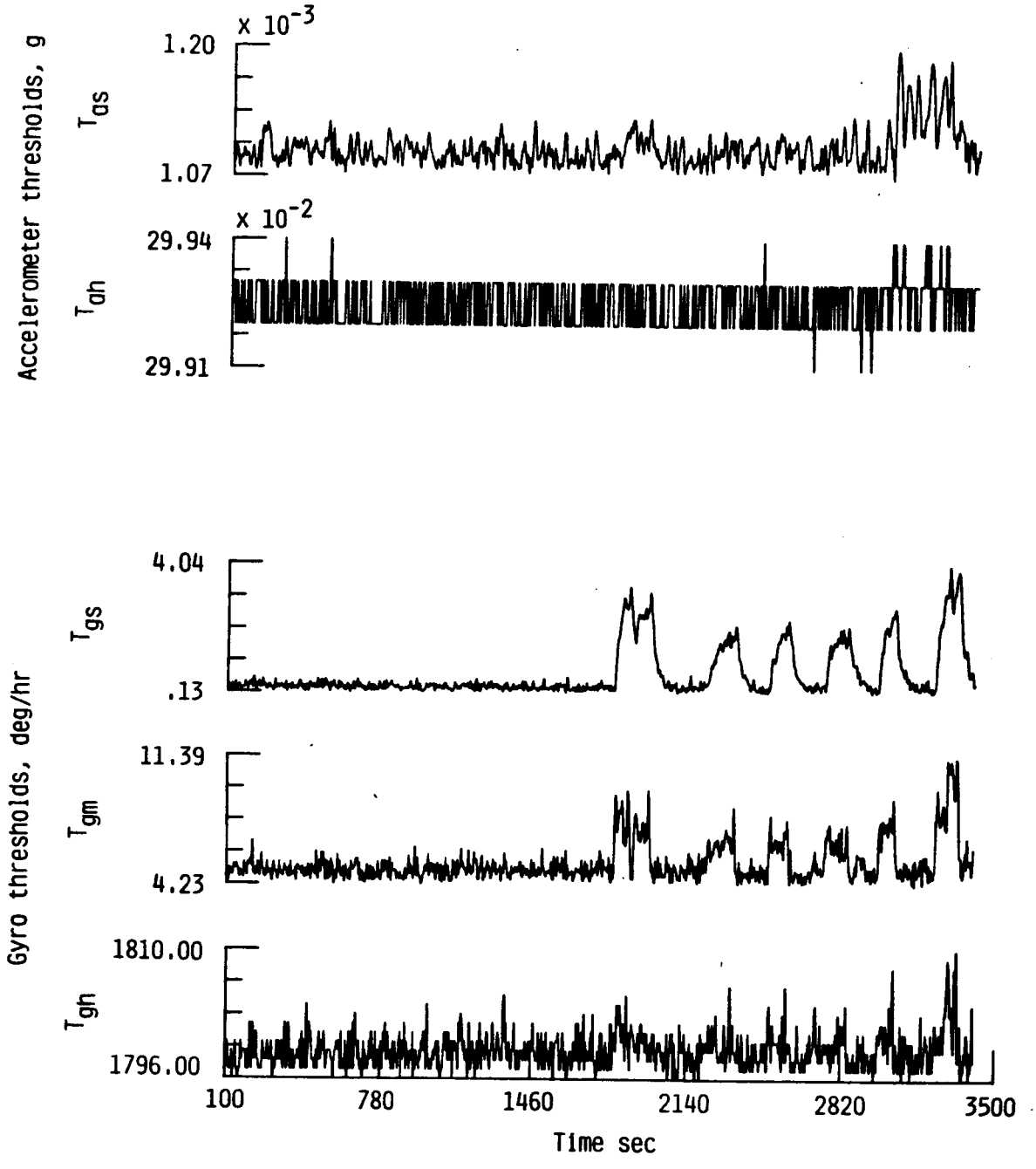

Figure 12. Gyro and accelerometer threshold functions for evaluation trajectory.

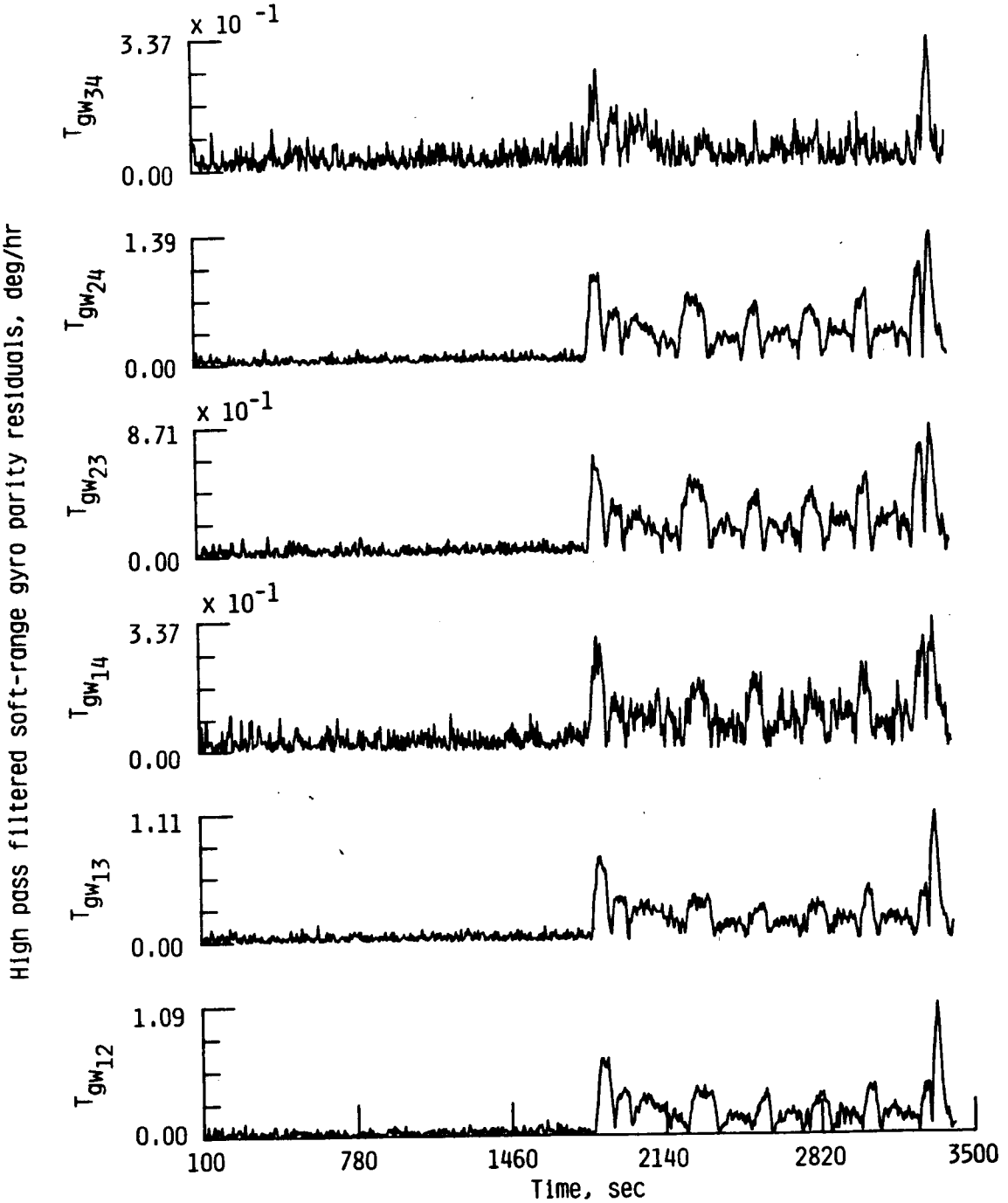

Figure 13. Washout filter response to evaluation trajectory for soft-range gyro parity residuals.

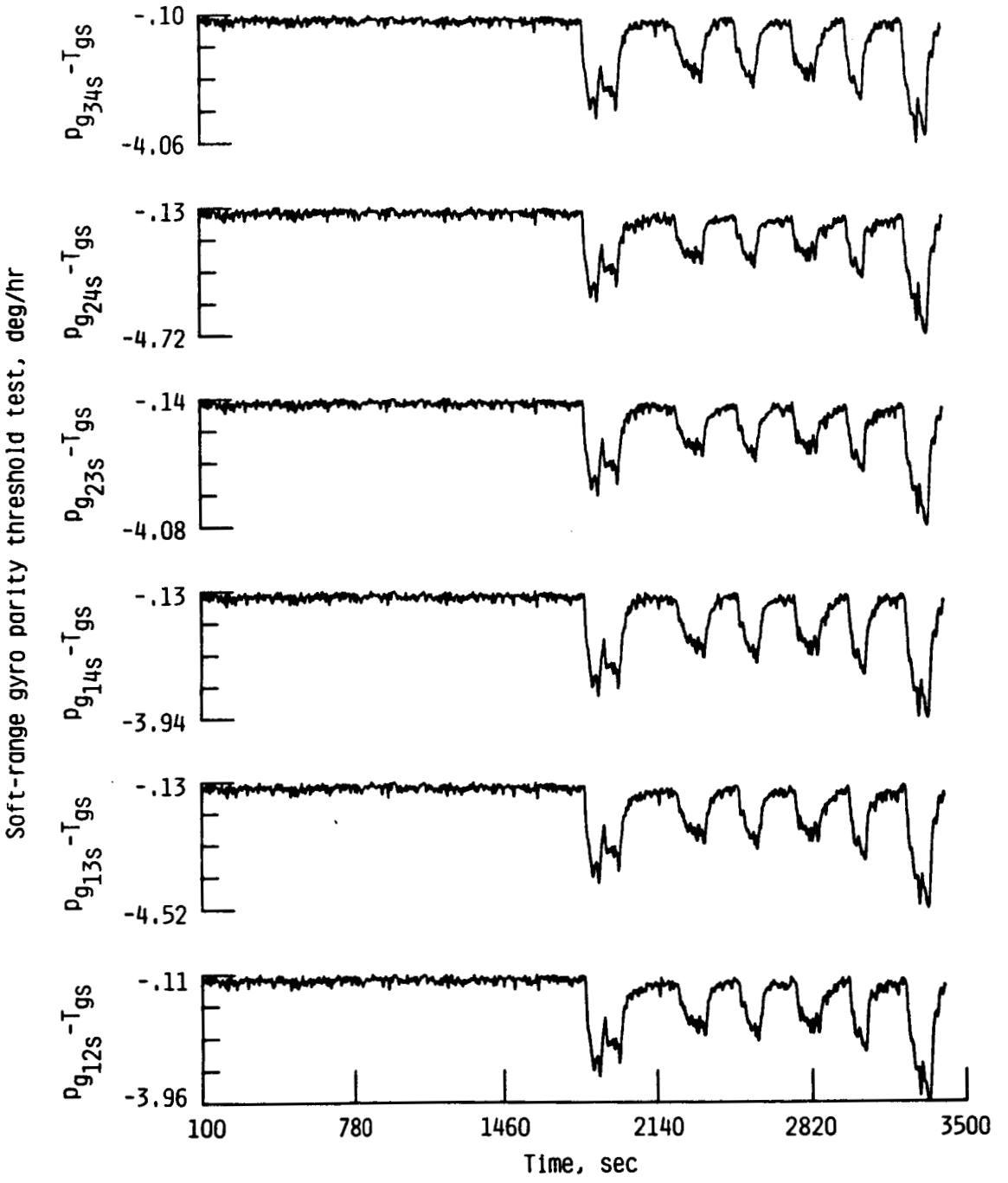

Figure 14. Threshold test results for soft-range gyro parity residuals.

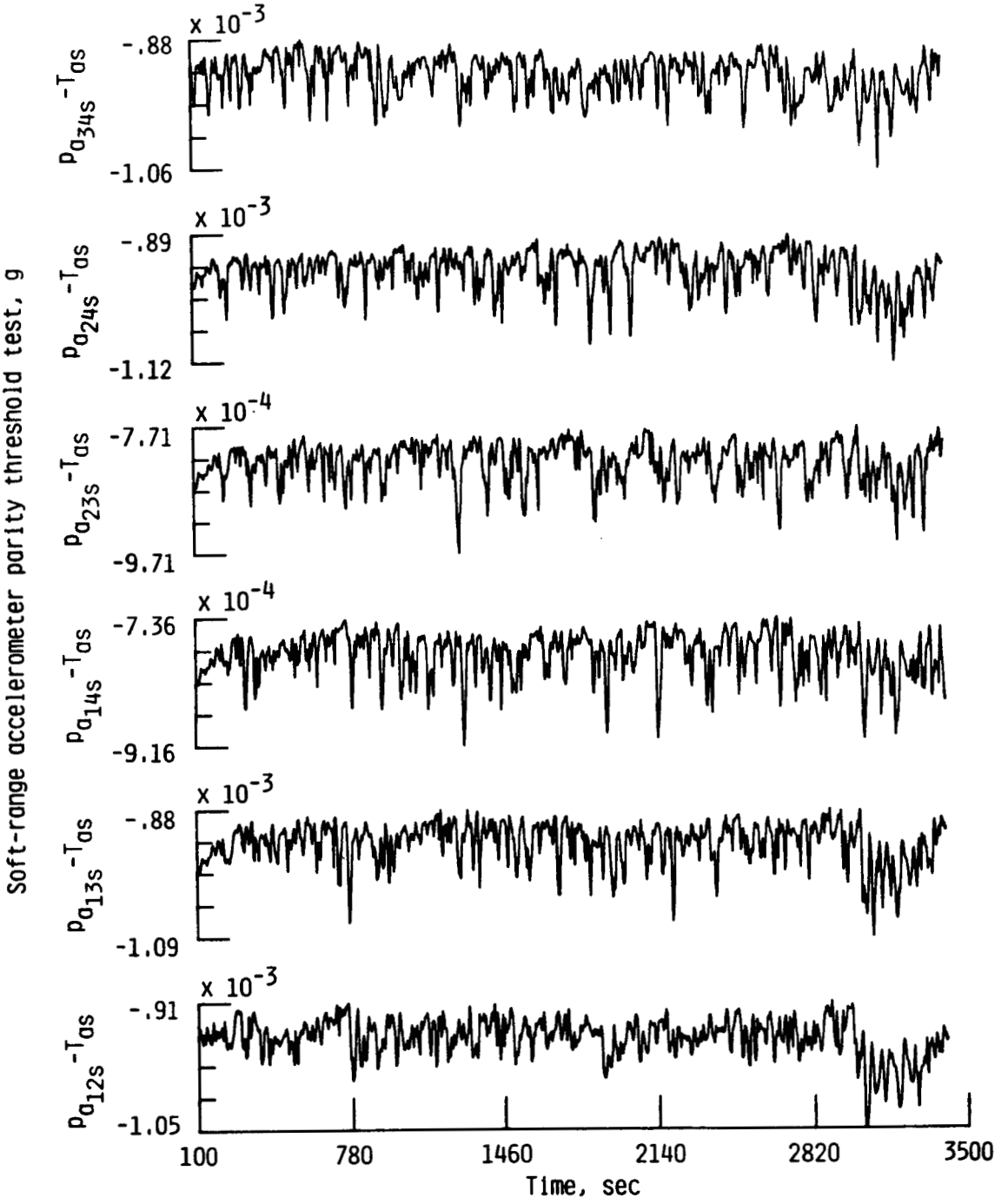

Figure 15. Threshold test results for soft-range accelerometer parity residuals.

1. Report No.	2. Government Accession No.	3. Recipient's Catalog No.
NASA TM-100493		

4. Title and Subtitle	5. Report Date
A VECTOR-BASED FAILURE DETECTION AND ISOLATION ALGORITHM FOR A DUAL FAIL-OPERATIONAL REDUNDANT STRAPDOWN INERTIAL MEASUREMENT UNIT	September 1987
	6. Performing Organization Code
7. Author(s)	8. Performing Organization Report No.
Frederick R. Morrell and Melvin L. Bailey*	
	10. Work Unit No.
9. Performing Organization Name and Address	505-66-21-06
NASA Langley Research Center Hampton, VA 23665-5225	11. Contract or Grant No.
	13. Type of Report and Period Covered
12. Sponsoring Agency Name and Address	TECHNICAL MEMORANDUM
National Aeronautics and Space Administration Washington, DC 20546	14. Sponsoring Agency Code

15. Supplementary Notes

*PRC Kentron Inc.
Hampton, VA

16. Abstract

A vector-based failure detection and isolation technique for a skewed array of two degree-of-freedom inertial sensors is developed. Failure detection is based on comparison of parity equations with a threshold, and isolation is based on comparison of logic variables which are keyed to pass/fail results of the parity test. A multi-level approach to failure detection is used to ensure adequate coverage for the flight control, display, and navigation avionics functions. Sensor error models are introduced to expose the susceptibility of the parity equations to sensor errors and physical separation effects. The algorithm is evaluated in a simulation of a commercial transport operating in a range of light to severe turbulence environments. A bias-jump failure level of 0.2 deg/hr was detected adn isolated properly in the light and moderate turbulence environments, but not detected in the extreme turbulence environment. An accelerometer bias-jump failure level of 1.5 milli-g was detected over all turbulence environments. For both types of inertial sensor, hard-over, and null type failures were detected in all environments without incident. The algorithm functioned without false alarm or isolation over all turbulence environments for the runs tested.

17. Key Words (Suggested by Author(s))	18. Distribution Statement
fault tolerance inertial sensors Inertial Measurement Unit reliability	UNCLASSIFIED - UNLIMITED Subject Category - 06

19. Security Classif. (of this report)	20. Security Classif. (of this page)	21. No. of Pages	22. Price
UNCLASSIFIED	UNCLASSIFIED	45	A03

For sale by the National Technical Information Service, Springfield, Virginia 22161